

ISSN 1732-9353 (suspended)
eISSN 2543-7496

Scientific Review

Engineering and Environmental Sciences

Przegląd Naukowy
Inżynieria i Kształtowanie Środowiska

Vol. 31 (2)

2022
Quarterly

Issue 96

SCIENTIFIC REVIEW
ENGINEERING AND ENVIRONMENTAL SCIENCES

Quarterly

EDITORIAL BOARD

Kazimierz Adamowski (University of Ottawa, Canada), **Kazimierz Banasik – Chairman** (Warsaw University of Life Sciences – SGGW, Poland), Andrzej Ciepiewski (Warsaw University of Life Sciences – SGGW, Poland), Tomáš Dostál (Czech Technical University in Prague, Czech Republic), Vidmantas Gurklys (Aleksandras Stulginskis University, Kaunas, Lithuania), Małgorzata Gutry-Korycka (University of Warsaw, Poland), Zbigniew Heidrich (Warsaw University of Technology, Poland), Silvia Kohnova (Slovak University of Technology, Bratislava, Slovak Republic), Andrzej J. Kosicki (Maryland State Highway Administration, Baltimore, USA), Hyosang Lee (Chungbuk National University, Korea), Athanasios Loukas (University of Thessaly, Volos, Greece), Jurík Luboš (Slovak Agriculture University, Nitra, Slovak Republic), Viktor Moshynskyi (National University of Water Management and Nature Resources Use, Rivne, Ukraine), Magdalena Daria Vaverková (Mendel University in Brno, Czech Republic)

EDITORIAL OFFICE

Tomasz Gnatowski (Deputy-chairman), Weronika Kowalik, Paweł Marcinkowski (Editorial Assistant Environmental Sciences), Katarzyna Pawluk, **Mieczysław Połoński (Chairman)**, Magdalena Daria Vaverková, Grzegorz Wierzbicki, Grzegorz Wrzesiński (Editorial Assistant Engineering Sciences)

The list of reviewers is published in the last issue of the volume and on the <https://srees.sggw.edu.pl>

EDITORIAL OFFICE ADDRESS

Wydział Budownictwa i Inżynierii Środowiska SGGW, ul. Nowoursynowska 159, 02-776 Warsaw, Poland
tel. (+48 22) 59 35 363, 59 35 210, 59 35 302
e-mail: srees@sggw.edu.pl
<https://srees.sggw.edu.pl>

ISSN 1732-9353 (suspended)
e-ISSN 2543-7496

Electronic version of the Scientific Review Engineering and Environmental Sciences is primary version

All papers are indexed in the data bases as follows: AGRO(Poznań), BazTech, Biblioteka Nauki, **CrossRef**, **DOAJ**, **Google Scholar**, **Index Copernicus**, INFONA, POL-Index, **SCOPUS**, SIGZ(CBR)

Scientific Review

Engineering and Environmental Sciences

Przegląd Naukowy
Inżynieria i Kształtowanie Środowiska

Vol. 31 (2)

2022

Issue 96

Contents

ABDULLAH M.D., MUHAISIN M.H. AMMASH H.K.: Effect of shear span-to-depth ratio on behavior of sandwich core steel girder with corrugated web	79
ELHAWARY E.I.N., ELSAFOURY A.H., AHMAD S.S.E. Durability of hybrid fiber reinforced concrete at various environmental media	88
ALI S., ALALIKHAN A. Enhancing the flexural load capacity of the reinforced concrete simply supported slabs using damaged tires strips (DTS)	101
VÍTKOVÁ E., VAŇKOVÁ L., OBLOUKOVÁ A.: Comparison of the price level of the water and sewerage charge rates and macroeconomic indicators in the Czech Republic	113
WAN KAMARUDIN W.F., IRWAN Z., YAAFAR M.R., MAT AMIN A.R.: Lockdown effect on carbon monoxide concentration over Malaysia and Indonesia	124
SLIMANI H., ABDI A., BRANES Z.: Isolation, characterization and growth assessment of biodegrading chlorpyrifos-methyl <i>Bacillus</i> species isolated from Algerian soil	135

Wydawnictwo SGGW, Warsaw 2022

Editorial work – Anna Dołomisiewicz, Violetta Kaska

ISSN 1732-9353 (suspended) eISSN 2543-7496

Mazin D. ABDULLAH¹

Muthana H. MUHAISIN²✉  <https://orcid.org/0000-0003-4581-9098>

Haider K. AMMASH²  <https://orcid.org/0000-0003-3672-6295>

¹ University of Al-Basrah, College of Engineering, Iraq

² University of Al-Qadisiyah, College of Engineering, Iraq

EFFECT OF SHEAR SPAN-TO-DEPTH RATIO ON BEHAVIOR OF SANDWICH CORE STEEL GIRDER WITH CORRUGATED WEB

Key words: steel beam, shear span, corrugated web, sandwich core, experimental results

Introduction

Corrugated steel girders are typically comprised from upper and lower flanges connected by corrugated steel webs. Using the corrugated web in lieu of the flat web in girders modifies the behavior of the system, resulting in several desirable features. Extensive research has been conducted during the last 30 years to explore the response of members with corrugated webs (Hamilton, 1993; Elgaaly, Hamilton & Seshadri, 1996; Abbas, Sause & Driver, 2006; Driver, Abbas & Sause, 2006; Kadhim & Ammash, 2021). Many aspects were considered in these investigations, including the shear behavior,

the flexural behavior, the torsional behavior, the fatigue behavior and so on. The results of these studies showed that girders with corrugated steel webs have several advantages such as significant shear stability, high strength-to-weight ratio, eliminate the need for transfer stiffeners, long fatigue life, high out of plane stiffness, and lower cost compared to conventional steel web girders.

To accelerate the production speed of girders with corrugated webs, and to overcome the low efficiency of manual welding, robots have been utilized in the production process as shown in Figure 1 (Pasternak & Kubieniec, 2010; Ibrahim, 2015; Hassanein, Elkawas, Bock, Shao & Elchalakani, 2021). Three-dimensional printing has been also recently introduced in production process (Abureden, Hasan & Ababneh, 2021). Due to its favorable properties, girder with corrugated web has been increasingly used in

different type of structures such as, bridges, industrial buildings, airplane hangars, and hydraulic structures (He, Liu, Chen & Yoda, 2012; Aydın, Yuksel, Yardımcı & Gokce, 2016; Zhou, Liu, Wang & Fahmi Hassanein, 2020). During the last three decades, steel girders with corrugated webs have been widely exploited in several bridges constructed in different countries: Japan, France and China. Due to this widespread of exploiting the girders with corrugated web, the expectation that the conventional girders with flat web will vanish within the next few decades and will be taken over by girders with corrugated web (Hassanein & Kharoob, 2014; Ibrahim 2015). Figure 2 shows examples of structures constructed using corrugated steel web.

To further enhance the stiffness and strength of steel girders that constructed with corrugated webs, two plates (skins) may be added to the face and the back of the corrugated plate (web) to form a sandwich core. Experimental work conducted by Ammash and Al-Bader (2021) showed that girders with sandwich core web (corrugated web and skins) have higher load capacity than girders with corrugated web only.

Using steel girders with different shear span-to-depth ratios (a/d) and core thickness may have a significant impact on the ultimate load capacity and mode failure of such kind



FIGURE 1. Using robots in production process Pasternak and Kubieniec (2011)



FIGURE 2. Examples of structures constructed using corrugated steel web: a – Ilsun bridge (Jung, Yi & Kim, 2010); b – industrial building (Parys, 2017); c – column and girder in industrial building (adopted from Ibrahim, 2015); d – airplane hangar (adopted from Ibrahim, 2015)

of structures, since the responses the girders could be switched from shear control to flexural control. To the extent of our knowledge, there is no study has been conducted on effect of a/d and core thickness on the performance steel girders with sandwich core constructed with corrugated web. In this paper, the influences of a/d and core thickness on the performance of sandwich core steel girders with corrugated webs will be experimentally investigated and compared with conventional flat web girders.

Experimental work

A total of nine girder specimens with simple span were fabricated and tested under mid span concentrated force to investigate impacts of the shear span-to-depth ratio (a/d) and depth of the corrugation on the performance of core sandwich girders with corrugated web. The specimens are categories as follows:

- A – three specimens with flat web (FW),
- B – three specimens with sandwich core web that have 30 mm core depth (SCW30),
- C – three specimens with sandwich core web that have 60 mm core depth (SCW60).

Three shear span-to-depth ratios (a/d): 1, 1.833 and 2.5, were considered for each category. Two core depths (Fig. 3) were also examined. The section dimensions for each category were selected so all the beams have the same weight. Dimensions of the specimens are presented in Figure 4 and Table 1. Same materials were used for all the specimens (properties of material are provided in Table 2). The specimens were loaded in 2,000 kN capacity testing machine, one concentrated load at mid span was applied and gradually increased until failure. The testing machine was stopped at different load level to read the mid span deflection of the tested beam. Linear variable displacement

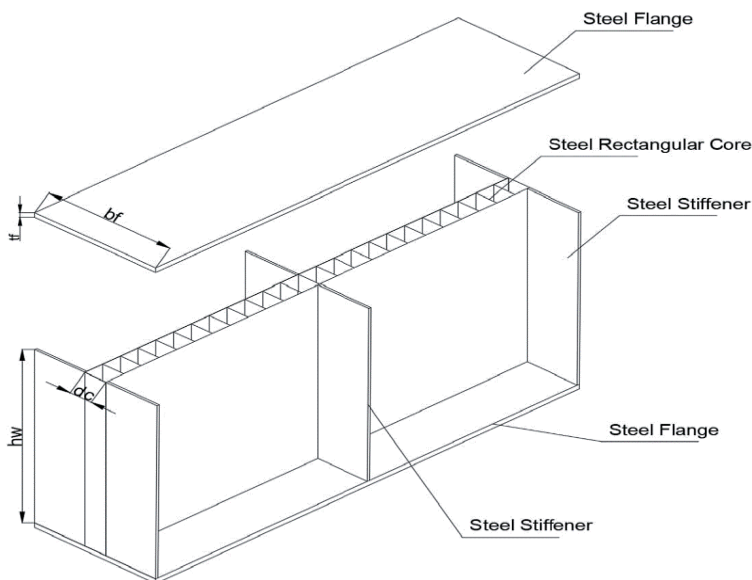


FIGURE 3. Details of the sandwich core web girder

TABLE 1. Dimensions of the tested beams

Group	Core thickness (d_c) [mm]	Span-to-depth ratio (a/d)	Flange width (b_f) [mm]	Flange thickness (t_f) [mm]	Web height (h_w) [mm]	Web thickness (t_w) [mm]	Corrugated thickness (t_c) [mm]	Skin thickness (t_s) [mm]	Span
A Flat web	-	1	200	6	300	3	-	-	600
		1.833	200	6	300	3	-	-	1 100
		2.5	200	6	300	3	-	-	1 500
B SCW30	30	1	200	6	300	-	1	1	600
		1.833	200	6	300	-	1	1	1 100
		2.5	200	6	300	-	1	1	1 500
C SCW60	60	1	200	6	300	-	1	1	600
		1.833	200	6	300	-	1	1	1 100
		2.5	200	6	300	-	1	1	1 500

TABLE 2. Material properties of the tested specimens

Element	Thickness (t) [mm]	Yield strength (F_y) [MPa]	Ultimate strength (F_u) [MPa]	Modulus of elasticity (E) [GPa]
Flange/stiffener	6	358	467	205
Flat web	3	402	455	203
Core sandwich web	corrugated web	410	206	206
	skin			

transducer (LVDT) deflection gauge was installed in mid span at the center of the bottom flange of each beam. To avoid bearing of the flanges, stiffeners with 300 mm width and 6 mm thickness were added to the both

side of the web (one under the load and the other at each support). Photos for specimen's preparation and testing setup are shown in Figure 5. Samples of the tested beams during testing are provided in Figure 6.

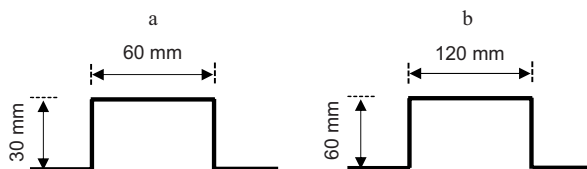


FIGURE 4. Rectangular web corrugation used in this study: a – SCW30; b – SCW60



FIGURE 5. Preparation of the specimens and test setup

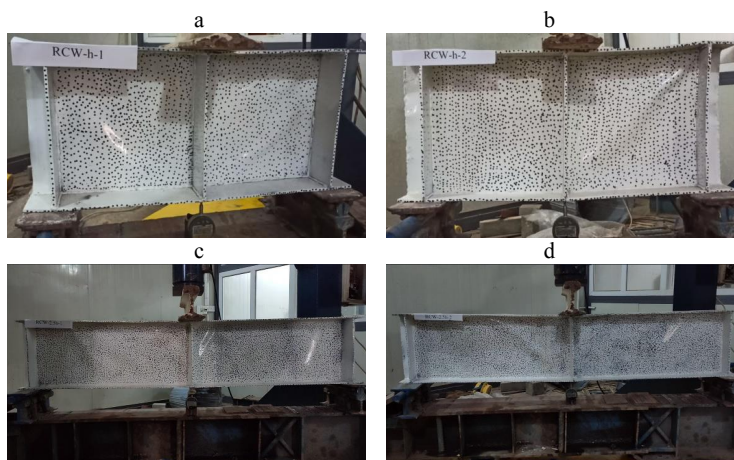


FIGURE 6. Girders with sandwich core during testing: a – SCW30 with $a/d = 1.0$; b – SCW60 with $a/d = 1.0$; c – SCW30 with $a/d = 2.5$; d – SCW60 with $a/d = 2.5$

Results and discussion

Figures 7–9 show the load–mid span deflection curves for girders with flat web, sandwich core web with 30 mm thick (SCW30), and sandwich core web with 60 mm thick (SCW60), respectively, at different a/d ratios. The relationship between ultimate load and a/d ratio for the three cases considered (flat web, SCW30 and SCW60) are shown in Figure 10. Figures 11–13 represent the load–mid span deflection curves for all the three types of webs considered at a/d equals to 1.0,

1.833 and 2.5 respectively. The ultimate load capacities for all the tested specimens are presented in Table 3.

Based on the results obtained from this study, the following notes can be observed.

- For the same a/d ratio, girders with sandwich core webs have higher ultimate load capacity than girders with flat web. At $a/d = 1.0$, the difference was about 44 and 20% for girders with web thickness of 30 and 60 mm respectively. This difference can be attributed to effect of corrugation in preventing the web local buckling.

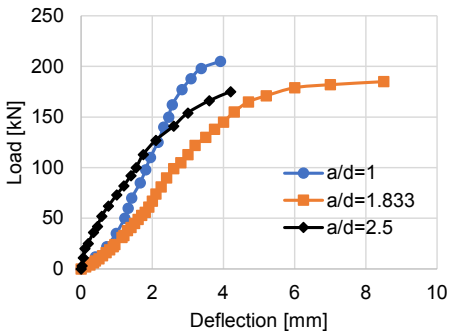


FIGURE 7. Load–mid span displacement curve for flat web with different a/d

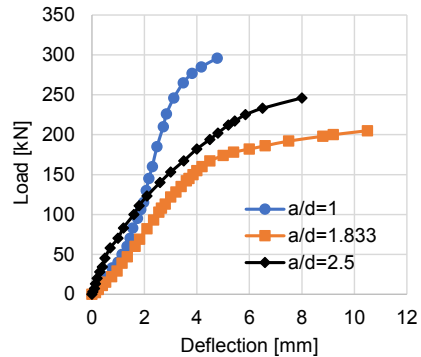


FIGURE 8. Load–mid span displacement curve for SCW30 with different a/d

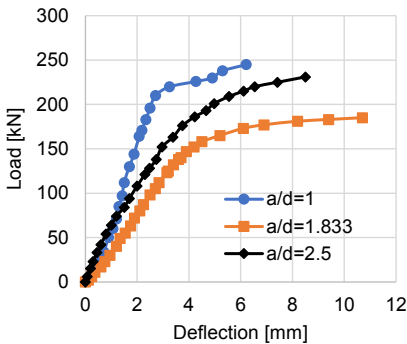


FIGURE 9. Load–mid span displacement curve for SCW60 with different a/d

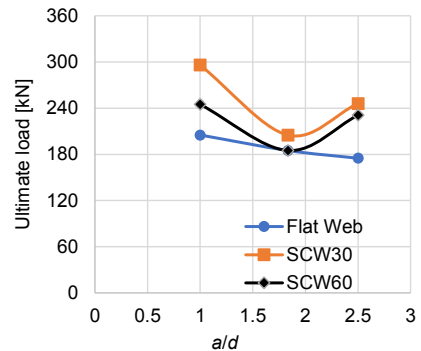


FIGURE 10. Ultimate load versus a/d ratio for flat web, SCW30 and SCW60

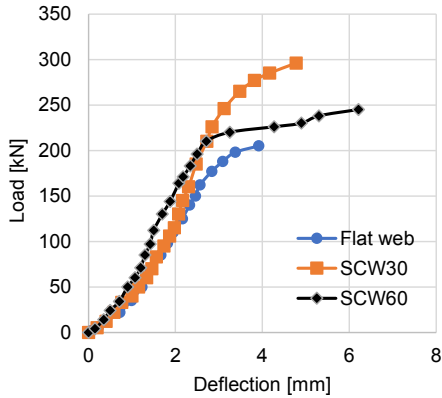


FIGURE 11. Load deflection curve for girders with flat web, SCW30 and SCW60 at $a/d = 1.0$

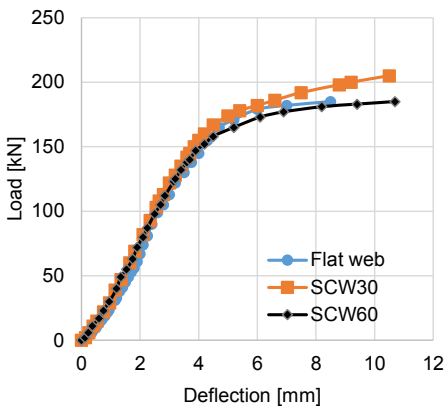


FIGURE 12. Load deflection curve for girders with flat web, SCW30 and SCW60 at $a/d = 1.833$

- Girders with sandwich core with web thickness of 30 mm (SCW30) have higher ultimate load capacity than girders with core thickness of 60 mm (SCW60), the

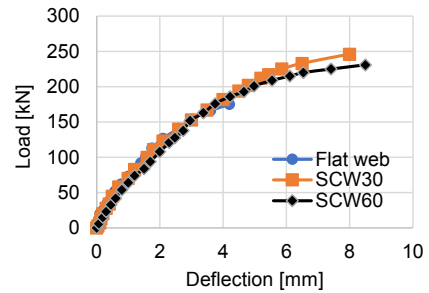


FIGURE 13. Load deflection curve for girders with flat web, SCW30 and SCW60 at $a/d = 2.5$

difference was about 20, 10 and 6% at a/d equals to 1.0, 1.833 and 2.5 respectively. This can be interpreted that the unsupported length of SCW60 is two times the unsupported length of SCW30 (as shown in Fig. 3), thus SCW60 is more suspected to local buckling than SCW30.

- For girders with flat web, the ultimate strength of specimens with a/d equals to 1.0 was about 8 and 17% higher than the corresponding strength for specimens with a/d equals to 1.833 and 2.5 respectively.
- The ultimate strength for girders with SCW30 at a/d equals to 1.0 was higher than the corresponding strength at a/d equals to 1.833 and 2.5 by about 44 and 20% respectively, while the ultimate strength for girders with SCW60 at a/d equals to 1.0 was higher by about 32 and 6%. The inconstancy of the results especially at a/d equals to 1.833 may be attributed to the effect of interaction between shear and flexure.

TABLE 3. Ultimate load capacities for the tested specimens

Span-to-depth ratio (a/d)	Ultimate load [kN]		
	flat web	sandwich core web	
		SCW30	SCW60
1.0	205	296	245
1.833	185	205	185
2.5	175	246	231

Conclusions

The impact of shear span-to-depth ratio and core thickness on the performance of sandwich core steel girders with corrugated web was investigated experimentally in this study. From the results of this work, the following observations were drawn.

- Sandwich core steel girders with corrugated web perform better than steel girders with flat web in term of both loading capacity and maximum displacement.
- The performance of the tested beams was noticeably affected by a/d ratio for all the categories considered in this study.
- For all the three categories (flat web, sandwich core with 30 mm thick, and sandwich core with 60 mm thick), girders with a/d equals to 1.0 perform better than girders with a/d equals to 1.833 and 2.5.
- Girders with sandwich core thickness of 30 mm demonstrate higher ultimate load capacity than girders with sandwich core of 60 mm, the maximum difference in the ultimate load capacity can be seen at a/d equals to 1.0.

References

- Abbas, H. H., Sause, R. & Driver, R. G. (2006). Behavior of corrugated web I-girders under in-plane loads. *Journal of Engineering Mechanics*, 132 (8), 806–814.
- Abureden, G. A., Hasan, W. M. & Ababneh, A. N. (2021). Exploring potential benefits of additive manufacturing in creating corrugated web steel beams. *Journal of Constructional Steel Research*, 187, 106975. <https://doi.org/10.1016/j.jcsr.2021.106975>
- Ammash, H. K. & Al-Bader, M. A. (2021). Shear behaviour of steel girder with web-corrugated core sandwich panels. *IOP Conference Series: Materials Science and Engineering*, 1090 (1), 012017. <https://doi.org/10.1088/1757-899X/1090/1/012017>
- Aydın, R., Yuksel, E., Yardımcı, N. & Gokce, T. (2016). Cyclic behaviour of diagonally-stiffened beam-to-column connections of corrugated-web I sections. *Engineering Structures*, 121, 120–135.
- Driver, R. G., Abbas, H. H. & Sause, R. (2006). Shear behavior of corrugated web bridge girders. *Journal of Structural Engineering*, 132 (2), 195–203.
- Elgaaly, M., Hamilton, R. W. & Seshadri, A. (1996). Shear strength of beams with corrugated webs. *Journal of Structural Engineering*, 122 (4), 390–398.
- Hamilton, R. W. (1993). *Behavior of welded girders with corrugated webs* (PhD thesis). University of Maine, Orono, ME.
- Hassanein, M. F., Elkawas, A. A., Bock, M., Shao, Y. B. & Elchalakani, M. (2021). Effect of using slender flanges on EN 1993-1-5 design model of mono-symmetric S460 corrugated web bridge girders. *Structures*, 33, 330–342.
- Hassanein, M. F. & Kharoob, O. F. (2014). Shear buckling behavior of tapered bridge girders with steel corrugated webs. *Engineering Structures*, 74, 157–169.
- He, J., Liu, Y., Chen, A. & Yoda, T. (2012). Mechanical behavior and analysis of composite bridges with corrugated steel webs: State-of-the-art. *International Journal of Steel Structures*, 12 (3), 321–338.
- Ibrahim, B. S. A. (2015). *Steel plate girders with corrugated webs. Past present and future*. Kair: Ain Shams University.
- Jung, K. H., Yi, J. W. & Kim, J. H. J. (2010). Structural safety and serviceability evaluations of prestressed concrete hybrid bridge girders with corrugated or steel truss web members. *Engineering Structures*, 32 (12), 3866–3878.
- Kadhim, A. W. & Ammash, H. K. (2021). Experimental study of encased composite corrugated steel webs under shear loading. *Journal of Physics: Conference Series*, 1895 (1), 012062. <https://doi.org/10.1088/1742-6596/1895/1/012062>
- Parys, A. (2017). *Primary structure, corrugated web beam*. Retrieved from: <https://primarystructure.net/corrugated-web-beam>

- Pasternak, H. & Kubieniec, G. (2010). Plate girders with corrugated webs. *Journal of Civil Engineering and Management*, 16 (2), 166–171.
- Zhou, M., Liu, Y., Wang, K. & Fahmi Hassanein, M. (2020). New asynchronous-pouring rapid-construction method for long-span prestressed concrete box girder bridges with corrugated steel webs. *Journal of Construction Engineering and Management*, 146 (2), 05019021. [https://doi.org/10.1061/\(ASCE\)CO.1943-7862.0001770](https://doi.org/10.1061/(ASCE)CO.1943-7862.0001770)

Summary

Effect of shear span-to-depth ratio on behavior of sandwich core steel girder with corrugated web. Girders with corrugated steel web are preferred and widely used in recently constructed bridges and industrial buildings. Sandwich core girders with corrugated web are constructed by adding two plates (skins) to the corrugated web. This study aims to in-

vestigate the shear span-to-depth ratio impact on the performance of sandwich core steel girders with corrugated web. Three span-to-depth ratios (a/d): 1.0, 1.833 and 2.5, were examined. The test includes three girders with sandwich web thickness of 30 mm, three girders with 60 mm sandwich web thickness, and three girders with conventional flat webs. A total of nine simply supported steel girders subjected to a concentrated load were fabricated and tested up to failure. The responses of the examined girders are presented in term of the load deflection curves, the ultimate load, and the maximum displacement. Among the conclusions drawn in this study that girders with sandwich core thickness of 30 mm demonstrate higher ultimate load capacity than girders with sandwich core of 60 mm, the maximum difference in the ultimate load capacity was about 20% and can be seen at a/d equals to 1.0. The results also pointed out that the behavior of the beams was noticeably impacted by the shear span-to-depth ratio.

DURABILITY OF HYBRID FIBER REINFORCED CONCRETE AT VARIOUS ENVIRONMENTAL MEDIA

Eslam Ibrahim Nasr ELHAWARY¹  <https://orcid.org/0000-0001-6516-2156>

Ashraf Hassan ELSAFOURY²  <https://orcid.org/0000-0001-6615-3083>

Seleem Saleh Elsayed AHMAD³  <https://orcid.org/0000-0001-9894-0209>

¹ Misr Higher Institute of Engineering and Technology, Egypt

² Zagazig Higher Institute of Engineering and Technology, Egypt

³ Zagazig University, Faculty of Engineering, Egypt

Key words: durability, hybrid fiber concrete, steel fibers, polypropylene fibers, compressive strength, splitting tensile strength, flexural strength

Introduction

The main objective of the research is to study the durability of hybrid concrete in various media. Reinforced concrete elements exposed to the sea environment have been studied by many researchers and found that concrete structure constructed in the ocean environment are severely eroded for many reasons before achieving their design service life. Some of them cracked over time and need to be repaired and some of them collapsed and need to be reconstructed due to the exposure of these facilities to sulphates and chlorides (Val & Stewart). Using normal concrete can-

not achieve the durability requirement for concrete structure in a harsh environment, therefore using special concrete that resists seawater and has long-life serviceability is recommended. Developing construction materials has generated a requirement for concrete with toughness, high strength, and durability. An example of durable concrete with strength is high-performance concrete reinforced with fiber which could be used to achieve mechanical properties compared with traditional concrete (Muigai, Moyo & Alexander, 2012; Kim, Hossain & Zhang, 2013; Cwirzen, Sztermen & Habermehl-Cwirzen, 2014; Demirel, Gultekin & Alyamaç, 2019). Some researchers studied the effect of hybridization for fibers on concrete properties. The main purpose of using hybrid fibers is to control different zones of cracking for concrete, at different size levels, at multiple loading, and various curing ages (Qian & Stroeven, 2000a).

Mohammadi, Singh and Kaushik (2008) investigated the influence of steel fiber additions with various aspect ratios on concrete compressive strength. With a volume proportion of 2%, two types of fibers were used: 65% long fiber and 35% short fiber. The splitting tensile strength of concrete was found to rise by up to 59%. Steel fibers of various lengths with fiber contents of 1.0, 1.5, and 2.0%. The results showed that compressive strength increased from 3 to 26% by using fiber. As observed in other studies, adding fiber led to a reduction in compressive strength as was observed in other studies (Bencardino, Rizzuti, Spadea & Swamy, 2008; Atiş & Karahan, 2009; Khitab et al., 2013). The main reason for the reduction in compressive strength is the dispersion of the fibers, especially in concretes with a high fiber content, which causes poor workability (Noushini, Samali & Vessalas, 2013). Dawood and Ramli (2011) experimented on high-strength mortar reinforced with hybrid fibers. It was found that hybrid fibers led to an increased modulus of elasticity by 52% for concrete. Yao, Li and Wu (2003) investigated the effect of low fibers volume fraction. Adding steel and carbon fibers led to an increase in splitting tensile strength, whereas using polypropylene fibers resulted in a reduction in indirect tensile strength. Hybridization of steel with carbon fibers resulted in high indirect tensile strength, this was superior to using steel or carbon fibers separately (Yu, Spiesz & Brouwers, 2014). Hybridization of two or more fibers with different types and sizes can improve more properties of concrete (Cattaneo & Biolzi, 2010; Yang, 2011; Banthia, Majdzadeh, Wu & Bindiganavile, 2014). Qian and Stroeven (2000b) evaluated the effect of adding different polypropylene

and steel fibers to reinforced specimens with fiber content ranging from 0.4 to 0.95% on flexural performance. In the small displacement range of hybrid fiber reinforced concrete, it was discovered that hooked end steel fiber $L = 40$ mm and $D = 0.3$ mm, as well as employed polypropylene fiber length $L = 12$ mm, had a substantial impact on load-bearing capacity. Sivakumar and Santhanam (2007) discovered that combining glass, polypropylene, or polyester fibers with steel fiber improved the performance of fiber reinforced concrete compared to concrete without fibers. Blunt and Ostertag (2009) have demonstrated that utilizing hybrid fibers significantly improved the flexural behavior of concrete when compared to a single fiber composite. The result of fiber hybridization led to increased flexural strength of up to 196% relative to the control specimens. Orouji, Zahrai and Najaf (2021) found that using 25% glass powder and 1.5% polypropylene fiber led to improves the compressive strength, flexural toughness, and ductility in the beams by about 1.6, 4, and 13.2 times, respectively.

Najaf, Orouji and Zahrai (2022) investigated the effect of waste glass powder, nanosilica, and recycled polypropylene fiber on lightweight concrete and they found that the best sample had 1.5% fiber, 3% nanosilica, and 25% waste glass powder, and had compressive and tensile strengths of roughly 1.7 and 1.6 times, respectively, those of the control specimen after 28 days.

Steel and polypropylene fibers are used in the experimental program. This paper investigated the mechanical properties with two-volume ratios subjected to four various media air, water, sodium chloride, and magnesium sulphate with a 7% concentration. In the present work, steel and polypropylene

fibers are used for hybrid performance, the mechanical properties of hybrid fiber concrete are being investigated subjected to four various media: air, water, sodium chloride, and magnesium sulphate with 7% concentration.

Experimental works

The most important purpose of this research is to experimentally study the durability of high performance fiber reinforced concrete with different types of fibers exposed to different environments like air, water, chlorides, and sulphates.

The evaluation of the effect of these environments is based on the mechanical properties of compressive, indirect tensile, and flexural tests. The experimental program includes the investigation of the durability of steel fiber concrete and polypropylene fiber concrete after exposure to these media for 28, 180, and 360 days.

Materials

Natural siliceous sand was used as a fine aggregate in the concrete mix with good quality and free from impurities. Physical properties of sand according to Egyptian code (Housing and Building National Research Center [HBNC], 2020) and sieve analysis of sand were determined (Tables 1 and 2).

The nominal maximum size of used dolomite was 14 mm as coarse aggregate. Physical properties of dolomite according to Egyptian code (HBNC, 2020) and sieve analysis of dolomite were determined (Tables 3 and 4). The dolomite was washed and immersed carefully in water to be fully saturated and then dried well over a sieve at room temperature before mixing.

TABLE 1. Physical properties of sand

Property	Measured value	Limit acc. to the ECP 203 standard (HBNC, 2020)
Compacted density [kg·m ⁻³]	1 795	–
Loose density [kg·m ⁻³]	1 700	–
Specific gravity	2.60	–
Fine material [%]	1.5	2.5

TABLE 2. Sieve analysis of sand

Sieve opening [mm]	Passing [%]	General limits
5	98.9	89–100
2.36	95.4	60–100
1.18	80.5	30–100
0.6	40.6	15–100
0.3	25.9	5–70
0.15	8.2	0–15

TABLE 3. Physical properties of dolomite

Property	Measured value	Limit acc. to the ECP 203 standard (HBNC, 2020)
Specific gravity	2.6	–
Unit weight [t·m ⁻³]	1.48	–
Absorption [%]	0.85	2
Organic materials [%]	none	0.05–0.1

TABLE 4. Sieve analysis of dolomite

Sieve opening [mm]	Passing [%]	General limits
50	100	–
37.5	100	–
20	100	–
14	98.1	85–100
10	40.5	0–50
5	3.8	0–10
2.36	0	–

Used water in all mixes was fresh water, free from impurities, and clean drinking water. The used water to cement ratio was 0.35 for all mixes. Portland cement CEM I with grade 52.5 N (producer Sinai White Portland Cement Company) was used in this work. Physical properties of used cement are illustrated in Table 5 according to Egyptian standard specifications (Egyptian Organization for Standardization and Quality Control [EOS], 2013).

TABLE 5. Physical properties of cement

Property	Test result	Value acc. to the ESS 4756-1 standard (EOS, 2013)
Specific gravity	3.15	–
Setting time		
initial [min]	90	≥ 45
final [h]	4.35	–
Fineness [cm ² ·g ⁻¹ ·m ⁻¹]	3 300*	–
Compressive strength after [MPa]		
2 days	30	≥ 20
28 days	65	≥ 52.5

*Sinai White Portland Cement Company results.

Silica fume had a particle size of 0.7 μm and a bulk density of 345 kg·m⁻³. Silica fume was added by a percentage of cement weight to the mix. It added 15% of the cement weight. A high range water reducer of the third generation called MasterGlenium® RMC 315 (producer BASF SE) with properties listed in Table 6 was used.

Hooked-end steel fiber used in this work is shown in Figure 1. Steel fiber has a length of 35 mm with a 0.8 mm diameter and modulus of elasticity of 200 GPa. The aspect ratio (L/D) was 43.75. The properties

of used steel fiber (supplier Nassar Group Egypt) are given in Table 7. Fiber volume fractions (V_f) of 0.5, 1, and 1.5% were used.

TABLE 6. Physical properties of MasterGlenium® RMC 315* (based on product data sheet)

Property	Value / Description
Appearance	off white opaque liquid
Specific gravity [g·cm ⁻³]	1.1
PH-value	6.5 ± 1
Alkali content [%]	≤ 2.00 by mass
Chloride content [%]	≤ 0.10 by mass
Air content	fulfilled
Water reduction [%]	≥ 112 of reference mix

*Certificate 0086-CPD-469071 EN 934-2: T3.1&T3.2.



FIGURE 1. Used steel fiber

TABLE 7. Properties of used steel fiber (based on product data sheet)

Property	Value / Description
Type	hooked end
Specific gravity	7.8
Tensile strength [MPa]	1 100
Crimped height [mm]	2.1–2.9
Length [mm]	35
Diameter [mm]	0.8
Aspect ratio	43.75

Polypropylene fiber is an additive fiber to reduce the occurrence of plastic shrinkage and plastic settlement cracking, whilst enhancing the surface properties and durability of hardened cementitious products.

It was supplied by the Sika AG as shown in Figure 2. The properties of used polypropylene fiber are given in Table 8. Fiber volume fraction (V_f) of 0.1, 0.3, and 0.5% were used.



FIGURE 2. Used polypropylene fiber

TABLE 8. Properties of used polypropylene fiber (based on product data sheet)

Property	Value / Description
Type	SikaFiber®
Density [$\text{g}\cdot\text{m}^{-3}$ nominal]	0.91
Tensile strength [$\text{N}\cdot\text{mm}^{-2}$]	300–400
Length [mm]	18
Melt point [$^{\circ}\text{C}$]	160
Specific surface area [$\text{m}^2\cdot\text{kg}^{-1}$]	250
Modulus of elasticity [$\text{N}\cdot\text{mm}^{-2}$]	4 000

Mix proportion and design

The mix proportions of all test specimens were given in Table 9 by using the absolute volume method. The fibers were added to the mix as a ratio of their volume by the

percentages illustrated in the experimental program and silica fume was added as a percentage of cement weight.

TABLE 9. Mix proportions of tested specimens

Mix items	Amount	Ratio
Cement	$500 \text{ kg}\cdot\text{m}^{-3}$	1
Silica fume	$75 \text{ kg}\cdot\text{m}^{-3}$	
Sand	$750 \text{ kg}\cdot\text{m}^{-3}$	1.31
Dolomite	$1\,000 \text{ kg}\cdot\text{m}^{-3}$	1.74
Water	$201 \text{ l}\cdot\text{m}^{-3}$	0.35
Superplasticizer	$10 \text{ l}\cdot\text{m}^{-3}$	0.017

Specimens details, mixing, curing, and testing

In this study cubic specimens with dimensions $100 \times 100 \times 100 \text{ mm}$ were cast for a compression test, for indirect tension testing, cylinder specimens with a diameter of 100 mm and a height of 200 mm were used, and beam specimens with dimensions of $100 \times 100 \times 500 \text{ mm}$ were used for flexural load testing with two loads at third points over a simply supported span of 400 mm. The basic elements were initially blended without fibers for the creation of this concrete. To avoid fiber balling and generate concrete with a homogeneous material consistency and good workability, the fibers were added in modest amounts. Then compacted on a vibration table. In this work, the slump test was used to determine the workability of the concrete mix. There's no indication of segregation, and the mixture was homogeneous and cohesive. It was observed that using fiber decreases the value of the slump than control specimens.

The specimens were demolded after 24 h from the time of casting and cured in tap water for 28-days at room temperature

conditions. After that specimens were placed in different media for a period of 28, 180 and 360 days. Those media were prepared as follows: water media consists of basins filled with drinking water, air media is at room temperature on the ground, the sulphate media consists of basins containing solutions of 7% magnesium sulphate, and the chloride media consists of basins containing solutions of 7% sodium chloride. The solution was changed after three months to keep constant concentration during the storage duration. The mechanical characteristics of specimens were measured using three standard tests. The machine is employed as a universal testing machine with a maximum capacity of 1,000 kN. The test setup for compressive strength, indirect tensile strength, and flexural strength, according to ASTM C496-96, ASTM C109/C109M-16, and ASTM C78/C78M-22 (ASTM International [ASTM], 1996; 2016; 2022), was shown in Figures 3, 4, and 5, respectively.



FIGURE 3. Compressive strength test



FIGURE 4. Indirect tensile strength test



FIGURE 5. Flexural strength test

Results and discussion

Compressive strength

The results showed that employing hybrid fiber with the addition of admixtures such as silica fume and superplasticizer increased concrete's compressive strength. The efficiency of additives in improving strength increased at early curing ages, as seen in Figure 6. When compared to control specimens, the average 28- and 180-day compressive strength of hybrid fiber concrete improved by 15.7 and 9.2%, respectively. This improvement is clearly when concrete is cured in clean water.

Compressive strength can also be illustrated in Figure 6, slightly improved after 360 days compared to 180 days' specimens' results.

According to the compressive test results obtained in this study, using hybrid fiber has a significant effect on compressive strength, which is likely due to an increase in mechanical bond strength when the fibers allow the formation of micro-cracks to be delayed and their propagation to be stopped to some extent. The effect of air, chloride, and sulphate

media on the compressive strength at 28, 180, and 360 days for control and hybrid fiber concrete were given, also, in Figure 6 as follows: Compressive strength for control specimens, in air media, at 28, 180 and 360 days were decreased from 72.84 to 72.30, from 78.75 to 78.13, and from 80.65 to 79.75 MPa, respectively, as compared to water media. Compressive strength

for control specimens, in chloride media, at 28, 180, and 360 days was decreased from 72.84 to 70.90, from 78.75 to 76.50, and from 80.65 to 77.25 MPa, respectively, as compared to water media.

The need for concrete replacement will be evaluated by a series of tests, including a water absorption test, a density test, and a compression strength test.

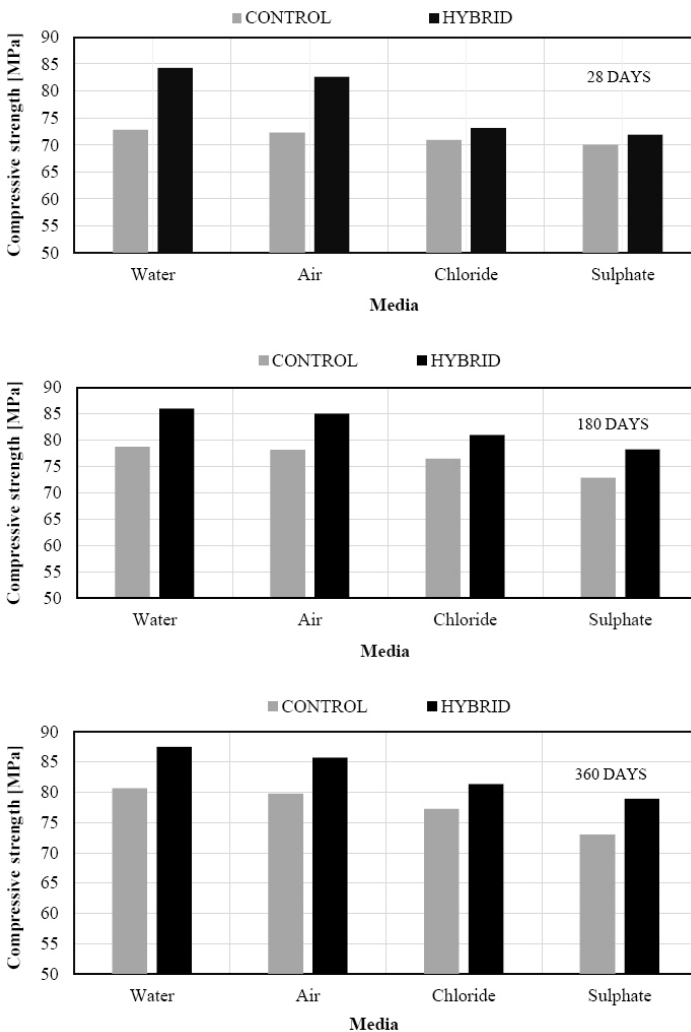


FIGURE 6. Compressive strength against curing media at different curing times for control and hybrid fiber reinforced concrete specimens

Compressive strength for control specimens, in sulphate media, at 28, 180 and 360 days were decreased from 72.84 to 70.05, from 78.75 to 72.83, and from 80.65 to 73 MPa, respectively, as compared to water media. These results clearly show there is little effect on compressive strength in air media and a severe effect on compressive strength in sulphate media.

Compressive strength for hybrid concrete specimens, in air media, at 28, 180 and 360 days were decreased from 84.3 to 82.63, from 86 to 85.03, and from 87.5 to 85.7 MPa, respectively, as compared to water media. Compressive strength for hybrid concrete specimens, in chloride media, at 28, 180 and 360 days were decreased from 84.3 to 73.13, from 86 to 80.97, and from 87.5 to 81.3 MPa, respectively, as compared to water media.

Compressive strength for hybrid concrete specimens in sulphate media at 28, 180 and 360 days decreased from 84.3 to 71.91, from 86 to 78.25, and from 87.5 to 78.9 MPa, respectively, as compared to water media. These results clearly show there is little effect on compressive strength in air media and a severe effect on compressive strength in sulphate media. On the other hand, the hybrid fiber concrete was more affected by aggressive media than the control specimen.

Flexural strength

The flexural strengths for hybrid fiber reinforced concrete containing steel and polypropylene fiber increased by 52.2, 13.9, and 17.4%, respectively, after 28, 180, and 360 days with respect to control specimens. This improvement is has occurred when concrete is cured in water media, as shown in Figure 7. From the obtained results in this research, increasing flexural strength is likely related to improvements in concrete's

toughness matrix, compactness, and fiber distribution homogeneity. This result is in agreement with the results of Blunt and Ostertag (2009) where they found that hybridization led to an increased flexural strength of up to 196% relative to the control specimens.

It can be seen in Figure 7 that the effect of air, chloride, and sulphate media on the flexural for control and hybrid fiber concrete. Flexural strength in air media, at 28, 180, and 360 days decreased from 6.15 to 5.88, from 8.72 to 7.68, and from 15.50 to 13.00 MPa, respectively, as compared to water media. Flexural strength for control specimens, in chloride media, at 28, 180, and 360 days decreased from 6.15 to 5.25, from 8.72 to 6.02, and from 15.50 to 11.00 MPa, respectively, as compared to water media. Flexural strength for control specimens, in sulphate media, at 28, 180, and 360 days were decreased from 6.15 to 5.14, from 8.72 to 6.24, and from 15.50 to 10.50 MPa, respectively, as compared to water media. These results clearly show there is little effect on flexural strength in air media and a severe effect on flexural strength in sulphate media. Flexural strength for hybrid concrete specimens, in air media, at 28, 180, and 360 days were decreased from 9.36 to 9.07, from 9.93 to 9.75, and from 18.20 to 16.40 MPa, respectively, as compared to water media. Flexural strength for hybrid concrete specimens, in chloride media, at 28, 180, and 360 days decreased from 9.36 to 8.57, from 9.93 to 8.80, and from 18.20 to 14.50 MPa, respectively, as compared to water media. Flexural strength for hybrid concrete specimens, in sulphate media, at 28, 180, and 360 days decreased from 9.36 to 7.86, from 9.93 to 8.42, and from 18.20 to 13.00 MPa, respectively, as compared to water media. These results clearly show

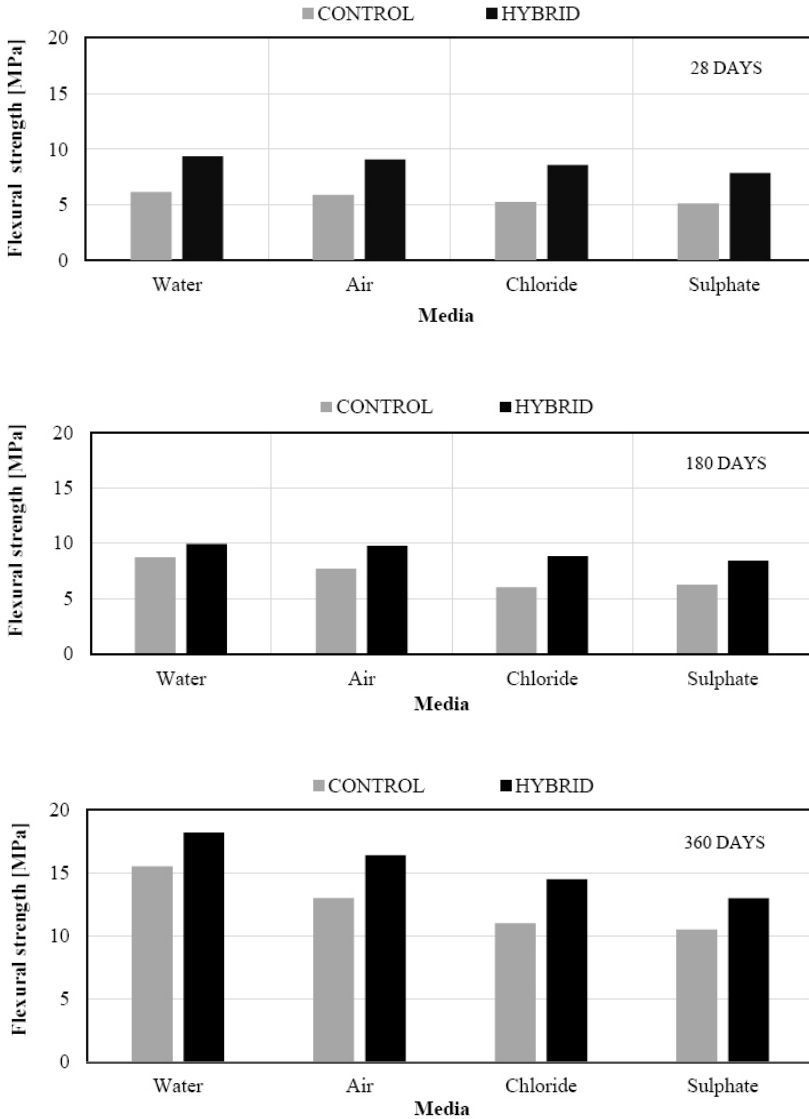


FIGURE 7. Flexural strength against curing media at different curing times for control and hybrid fiber reinforced concrete specimens

there is a little effect on flexural strength in air media and a severe effect on flexural strength in sulphate media. On the other hand, the hybrid fiber concrete was more affected by aggressive media than the control specimen.

Indirect tensile strength

The hybrid fiber reinforced concrete has a great influence on indirect tensile strength as shown in Figure 8. For different media, indirect tensile strength increased over time,

up to 360 days. The indirect tensile strength for hybrid fiber reinforced concrete has reached the maximum value of 16.5, 16.8, 15.2, and 14.8 MPa compared to control specimens for water, air, chloride, and sulphate, respectively, after 360 days.

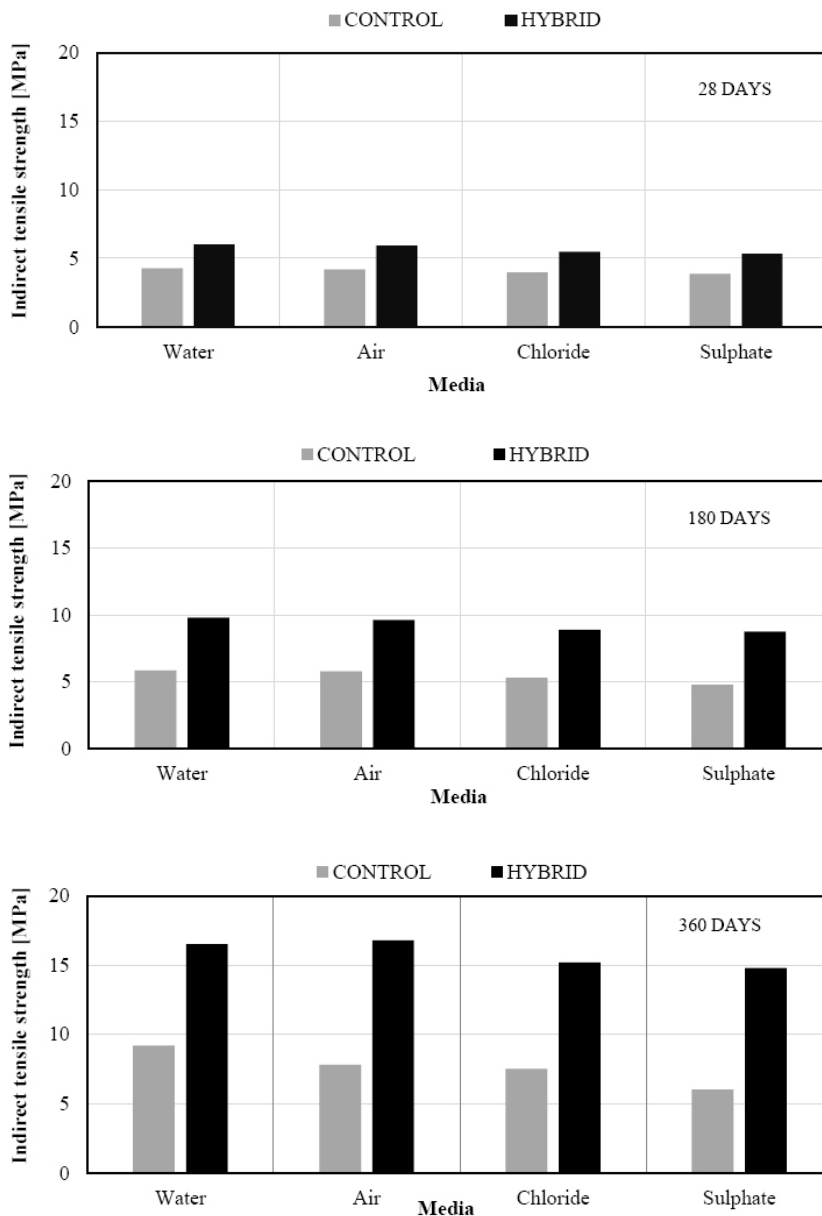


FIGURE 8. Indirect tensile strength against curing media at different curing times for control and hybrid fiber reinforced concrete specimens

From the results, using hybrid fiber reinforced concrete led to improve indirect tensile strength over time due to bonding between concrete and fiber, which made it withstand the toughest environmental conditions.

The effect of air, chloride, and sulphate media on the indirect tensile strength at 28, 180, and 360 days for control and hybrid fiber concrete was given, also, in Figure 8 as follows. Indirect tensile strength for control specimens, in air media, at 28, 180 and 360 days were decreased from 4.27 to 4.19, from 5.85 to 5.75, and from 9.20 to 7.80 MPa, respectively as compared to water media. Indirect tensile strength for control specimens, in chloride media, at 28, 180 and 360 days decreased from 4.27 to 3.95, from 5.85 to 5.28, and from 9.20 to 7.50 MPa, respectively, as compared to water media. Indirect tensile strength for control specimens, in sulphate media, at 28, 180 and 360 days decreased from 4.27 to 3.85, from 5.85 to 4.78, and from 9.20 to 6.00 MPa, respectively, as compared to water media.

These results clearly show there is little effect on indirect tensile strength in air media and a severe effect on indirect tensile strength in sulphate media. Indirect tensile strength for hybrid concrete specimens, in air media, at 28, 180 and 360 days decreased from 5.99 to 5.92, from 9.79 to 9.62, and from 16.50 to 16.40 MPa, respectively, as compared to water media. Indirect tensile strength for hybrid concrete specimens, in chloride media, at 28, 180 and 360 days decreased from 5.99 to 5.46, from 9.79 to 8.87, and from 16.50 to 15.20 MPa, respectively, as compared to water media. Indirect tensile strength for hybrid concrete specimens, in sulphate media at 28, 180 and 360 days decreased from 5.99 to 5.32, from 9.79 to 8.74, and from 16.50 to 14.80 MPa, respectively, as compared to

water media. These results clearly show there is little effect on indirect tensile strength in air media and a severe effect on indirect tensile strength in sulphate media. On the other hand, the hybrid fiber concrete was more affected by aggressive media than the control specimen.

Conclusions

The following are the results of an experimental investigation on hybrid fiber reinforced concrete:

- Using hybrid fiber reinforced concrete improves compressive strength up to 360 days.
- After 360 days in water media, the maximum indirect tensile strength of hybrid fiber reinforced concrete increased by 79.3% compared to control specimens.
- The flexural strengths of hybrid fiber reinforced concrete improved at water media by 17.4% after 360 days.
- Water is the best media and gives maximum strength up to 360 days.
- Sulphate media is the most aggressive media for hybrid fiber reinforced concrete.

References

- ASTM International [ASTM] (1996). *Standard Test Method for Splitting Tensile Strength of Cylindrical Concrete Specimens* (ASTM C496-96). West Conshohocken, PA: ASTM International.
- ASTM International [ASTM] (2016). *Standard Test Method for Compressive Strength of Hydraulic Cement Mortars (Using 2-in. or [50-mm] Cube Specimens)* (ASTM C109/C109M-16). West Conshohocken, PA: ASTM International.

- ASTM International [ASTM] (2022). *Standard Test Method for Flexural Strength of Concrete (Using Simple Beam with Third-Point Loading)* (ASTM C78/C78M-22). West Conshohocken, PA: ASTM International.
- Atiş, C. D. & Karahan, O. (2009). Properties of steel fiber reinforced fly ash concrete. *Construction and Building Materials*, 23 (1), 392–399.
- Banthia, N., Majdzadeh, F., Wu, J. & Bindiganavile, V. (2014). Fiber synergy in Hybrid Fiber Reinforced Concrete (HyFRC) in flexure and direct shear. *Cement and Concrete Composites*, 48, 91–97.
- Bencardino, F., Rizzuti, L., Spadea, G. & Swamy, R. N. (2008). Stress-strain behavior of steel fiber-reinforced concrete in compression. *Journal of Materials in Civil Engineering*, 20 (3), 255–263.
- Blunt, J. D. & Ostertag, C. P. (2009). Deflection hardening and workability of hybrid fiber composites. *ACI Materials Journal*, 106 (3), 265–272.
- Cattaneo, S. & Biolzi, L. (2010). Assessment of thermal damage in hybrid fiber-reinforced concrete. *Journal of Materials in Civil Engineering*, 22 (9), 836–845.
- Cwirzen, A., Szttermen, P. & Habermehl-Cwirzen, K. (2014). Effect of Baltic seawater and binder type on frost durability of concrete. *Journal of Materials in Civil Engineering*, 26 (2), 283–287.
- Dawood, E. T. & Ramli, M. (2011). High strength characteristics of cement mortar reinforced with hybrid fibers. *Construction and Building Materials*, 25 (5), 2240–2247.
- Demirel, B., Gultekin, E. & Alyamaç, K. E. (2019). Performance of structural lightweight concrete containing metakaolin after elevated temperature. *KSCE Journal of Civil Engineering*, 23 (7), 2997–3004.
- Egyptian Organization for Standardization and Quality Control [EOS] (2013). Cement. Part 1: Composition, specifications and conformity criteria for common cements (ESS 4756-1). Cairo: Egyptian Organization for Standardization and Quality Control.
- Housing and Building National Research Center [HBNC] (2020). Egyptian code for design and construction of reinforced concrete structures (ECP 203). Cairo: Housing and Building National Research Center.
- Khitab, A., Arshad, M. T., Hussain, N., Tariq, K., Ali, S. A., Kazmi, S. M. S. & Munir, M. J. (2013). Concrete reinforced with 0.1 vol% of different synthetic fibers. *Life Science Journal*, 10 (12), 934–939.
- Kim, Y. J., Hossain, M. & Zhang, J. (2013). A probabilistic investigation into deterioration of CFRP – concrete interface in aggressive environments. *Construction and Building Materials*, 41, 49–59.
- Mohammadi, Y., Singh, S. P. & Kaushik, S. K. (2008). Properties of steel fibrous concrete containing mixed fibres in fresh and hardened state. *Construction and Building Materials*, 22 (5), 956–965.
- Muigai, R., Moyo, P. & Alexander, M. (2012). Durability design of reinforced concrete structures: a comparison of the use of durability indexes in the deemed-to-satisfy approach and the full-probabilistic approach. *Materials and Structures*, 45 (8), 1233–1244.
- Najaf, E., Orouji, M. & Zahrai, S. M. (2022). Improving nonlinear behavior and tensile and compressive strengths of sustainable lightweight concrete using waste glass powder, nanosilica, and recycled polypropylene fiber. *Nonlinear Engineering*, 11 (1), 58–70.
- Noushini, A., Samali, B. & Vessalas, K. (2013). Effect of polyvinyl alcohol (PVA) fiber on dynamic and material properties of fiber reinforced concrete. *Construction and Building Materials*, 49, 374–383.]
- Orouji, M., Zahrai, S. M. & Najaf, E. (2021). Effect of glass powder & polypropylene fibers on compressive and flexural strengths, toughness and ductility of concrete: an environmental approach. *Structures*, 33, 4616–4628.
- Qian, C. X. & Stroeven, P. (2000a). Development of hybrid polypropylene-steel fiber-reinforced concrete. *Cement and Concrete Research*, 30 (1), 63–69.]
- Qian, C. & Stroeven, P. (2000b). Fracture properties of concrete reinforced with steel–polypropylene hybrid fibers. *Cement and Concrete Composites*, 22 (5), 343–351.

- Sivakumar, A. & Santhanam, M. (2007). Mechanical properties of high strength concrete reinforced with metallic and non-metallic fibers. *Cement and Concrete Composites*, 29 (8), 603–608.
- Val, D. V. & Stewart, M. G. (2003). Life-cycle cost analysis of reinforced concrete structures in marine environments. *Structural Safety*, 25 (4), 343–362.
- Yang, K. H. (2011). Tests on concrete reinforced with hybrid or monolithic steel and polyvinyl alcohol fibers. *ACI Materials Journal*, 108 (6), 664–672.
- Yao, W., Li, J. & Wu, K. (2003). Mechanical properties of hybrid fiber-reinforced concrete at low fiber volume fraction. *Cement and Concrete Research*, 33 (1), 27–30.
- Yu, R., Spiesz, P. & Brouwers, H. J. H. (2014). Static properties and impact resistance of a green Ultra-High Performance Hybrid Fiber Reinforced Concrete (UHPHFRC): Experiments and modeling. *Construction and Building Materials*, 68, 158–171.

Summary

Durability of hybrid fiber reinforced concrete at various environmental media.

Fiber's addition to concrete mixture attracts researchers to determine the effect of fiber type on durability properties of hybrid performance concrete. In the present work, steel and polypropylene fibers are used in hybrid form in the experimental program. The objective of this paper is to investigate the mechanical properties of hybrid fiber reinforced concrete subjected to four various media: air, water, sodium chloride, and magnesium sulphate with a 7% concentration. The results showed that using hybrid fibers which consist of 1% steel fiber and 0.3% polypropylene fiber improved the compressive strength, splitting tensile strength, and flexural strength for different media for up to 360 days.

Saba ALI

Ahmed ALALIKHAN   <https://orcid.org/0000-0001-5752-7362>

University of Kufa, Faculty of Engineering, Iraq

ENHANCING THE FLEXURAL LOAD CAPACITY OF THE REINFORCED CONCRETE SIMPLY SUPPORTED SLABS USING DAMAGED TIRES STRIPS (DTS)

Key words: flexural strength, reinforced concrete slabs, damaged tires strips

Introduction

One of the most difficult and problematic waste materials is the used tires of vehicles (Elnour & Laz, 2014; Bulei, Todor, Heput & Kiss, 2018). The disposal of damaged vehicle tires in some countries is a problem of increasing significance due to the annually incessant accumulation of more than a hundred million tires which are treated by either burning, backfilling, storing or dumping illegally (Edil, Park & Kim, 2004; Garrick, 2005). All these procedures are not friendly environment solutions, for instance, the burning process of tires pollutes the air and dumping them wastes valuable land for storing. Also, they exhibit unfavored site vision,

host for the growing of mosquito larvae, fire risk, and generated harmful gases, such as carcinogens when stockpiled (Garrick, 2005; Simalti & Singh, 2021). Avoiding the continuous accumulation of damaged vehicle tires needs to develop novelty methods of recycling and reusing the used tires to dispose them safely and economically. The recycling process aims to exploit the advantages that available in the raw materials of the damaged vehicle tires characterized by unique properties such as tensile resistance, sound concealment, and high chemical absorption (Edil et al., 2004).

The objectivity of using the damaged tire strips as an additional reinforcement in the field of construction is to achieve two concepts, a clean environment and economic considerations. A clean environment is achieved by consuming the damaged vehicles tires accumulated in the societies while

the economic considerations are represented by reducing the consumption of raw materials, increasing the thermal insulation due to the existed rubber material and saving the cost of the recycling process by using damaged tires directly. Recycling of damaged vehicle tires requires, usually, either mechanical or thermal preparation processes to convert them into useful materials. In the mechanical process, the steel cords in the tires are pulled out by a punch-like mechanism in order to be shredded and the remaining steel could be extracted by magnetic separators. The mechanical process produces crumb rubber (rubber granules) and steel cords. The thermal (pyrolysis) recycling process technique, on the other hand, uses a thermochemical method to decompose the tire. This technique produces, in addition to steel, carbon black and oil (Sengul, 2016) which are not ambient friendly productions. Using the damaged vehicle tires in the structural field satisfies sustainability concept and economic considerations if they can be used to replace raw construction materials made from limited resources (Edil et al., 2004).

Various methods for recycling of scrap tires have been suggested since the 1940s (Cao, 2007). Recently, researchers have been interested by the optimal disposal of waste tires (Yildirim, 2007; Celik & Atiş, 2008) which may be recycled using modern technologies such as chipping tires and convalescing steel cords to extract the useful materials within the tire contents (Bdour & Al-Khalayleh, 2010). The extracted useful materials could be used in several aspects within the civil construction field. For instance, graded rubber particles obtained from damaged tires are used as aggregate in the concrete mix by the partially replacement of the coarse or fine natural aggregate (Habib, Yildirim & Eren, 2020; Sharaky, Mohamed, Torres & Emara,

2020). Other studies (Sengul, 2016; Simalti & Singh, 2021) have investigated the ability of using the extracted steel pieces obtained from the recycled tires as steel fibers to produce fibrous concrete instead of the commercial types of fibers. Also, recycled damaged tires in the form of powder material was introduced as a material that could be used to replace part of the cement content in the concrete mix (Li, Ruan & Zeng, 2014; Valente & Sibai, 2019). Another aspects, such as asphaltic concrete (Shu & Huang, 2014) or concrete walls (Cecich, Gonzales, Hoisaeter, Williams & Reddy, 1996) are cases that were investigated to consume the recycled damaged tires. In the structural field, the reinforced concrete one-way slabs (RCOWS) and the reinforced concrete two-way slabs (RCTWS) give the opportunity as suitable structural members to be reinforced with the damaged tires strips (DTS) as an additional reinforcement. The ability of extracting the damaged tires strips (DTS) from the original tire frame directly by using a simple mechanical method used in the present work provides a friendly-environment recycling method rather than methods adopted in literature which are themselves considered as pollution operations (Pilakoutas, Neocleous & Tlemat, 2004).

The flexural strength of the structural members is very significant in the design of any structure. So, the present work investigates the flexural behavior of the reinforced concrete one-way slabs (RCOWS) and the reinforced concrete two-way slabs (RCTWS) in simply supported condition based on experimental tests. For the tested specimens, the study investigates the ability of increasing the flexural strength capacity as well as reducing the central deflection due to the application of DTS as an innovative additional reinforcing material that is not used before for such purpose.

Material and methods

Adopted specimens and reinforcement

The investigation includes testing of two groups of structural members reinforced by the DTS as an additional reinforcement. Group one represents the reinforced concrete one-way slabs (RCOWS) models while group two includes the reinforced concrete two-way slabs (RCTWS) models. Eight adopted specimens were investigated within the first group being with dimensions of $2,000 \times 500 \times 110$ mm respectively represent length, width and thickness of the slab such that the effective span is 1,800 mm for each model, as illustrated in Figure 1.

All specimens of the RCOWS group consist of three $\varnothing 8$ mm steel bars spaced at 150 mm c/c, in tension zone while $\varnothing 8$ mm steel bars are used as a secondary reinforcement, for shrinkage and temperature, distributed along the length of the slab spaced at 250 mm c/c. For the RCTWS group, one test specimen reinforced by the DTS as a case study in addition to the control specimen were investigated with dimensions of $1,000 \times 1,000 \times 100$ mm respectively represent length, width and thickness of the

slab such that the effective span is 950 mm for each model, as shown in Figure 2. The main reinforcement of the RCTWS group is represented by a square steel mesh of $\varnothing 6$ mm of bars spaced at 150 mm in two directions for all specimens, as shown in Figure 2.

Adopted categories of the DTS

Based on the adopted RCOWS and RCTWS groups, DTS were prepared according to two categories. The first category, adopted in the RCOWS models, represents DTS with dimensions of 1,960 mm length, 200 mm width and 10 mm thickness while the second category has the dimensions of 960 mm length, 150 mm width and 10 mm thickness used in the case of RCTWS models. As a main component consists the tire frame, the steel-cord construction of the standard tire casing is $4@0.28$ mm (the cable is made up of four filaments) placed within $\pm 23^\circ$ inclination in the tire belt (Edeskär, 2004). It is expected that DTS have the ability to increase the ultimate flexural load capacity due to the existence of steel wire mesh within texture of the tires strip when they are fixed throughout the slab tension zone.

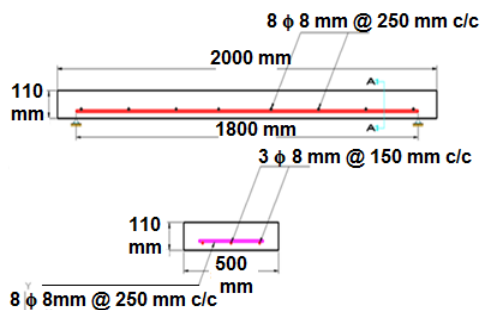


FIGURE 1. Details of the tested RCOWS control model

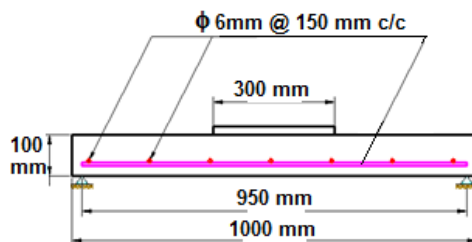


FIGURE 2. Details of tested RCTWS control model

Investigated parameters for the RCOWS and RCTWS models

In the present work, seven parameters have been studied for the RCOWS models representing seven cases of study, compared with one control specimen, while one case study is investigated for the RCTWS group in addition to the control specimen as following:

- Effect of using a single layer of DTS applied in the tension zone at zero elevation from the lower face of RCOWS model, identified as SOLS.
- Similar case study mentioned in the previous point is considered except that the DTS is applied at elevation of 25 mm from the lower face of the slab, identified as SOUS.
- Effect of using double layers of DTS applied such that the first layer being above the second layer (in vertical position) placed at elevation of 25 mm from the lower face of the RCOWS model, identified as SOUDV.
- Similar case study mentioned in the previous point is considered except that the two layers are placed within the same elevation (in horizontal position) at 25 mm from the lower face of the RCOWS model, identified as SOUDH.
- Three cases of study investigate the effect of overlapping distances as 50, 100

and 200 mm with respect to the flexural load capacity for the continuous DTS, in case when they are used for long spans, applied at elevation of 25 mm from the lower face of the RCOWS model, identified as SOUSO3, SOUSO1 and SOUSO2 respectively.

- The unique case study adopted for the RCTWS group is identified as STR which study the effect of using two layers of DTS, each layer contains three strips applied horizontally separated by 150 mm distance. The first layer is applied within the zero elevation (below the main steel reinforcement) in one direction of the RCTWS model while the second layer is placed in the elevation of 25 mm from the lower face (above the steel reinforcement) in the transverse direction with respect to the first layer. In this group, one model represents the control specimen identified as STC without DTS and another model represents the investigated case study reinforced with the DTS explained earlier.

Extracting and fixing process of the DTS

The DTS should be extracted first from the used tire using hand grinding machine to be as a layer that is able to be placed and fixed within the structural members throughout the tension zone, as shown in Figure 3.



FIGURE 3. Extracting the strips from the complete tire (Valente & Sibai, 2019)

Strip's fixing process represents the placing of each tire strip over the structural member, in the adequate position, without any separation between the contacted surfaces as much as possible. DTS have, usually, curvature tendency due to the original state that they were within the tire frame, as shown in Figure 3. Therefore, this behavior should be prevented during the fixing process of the DTS over the structural member by using steel nails. The steel nails are distributed each 100 mm along the slab length, to ensure that the strip is completely placed and fixed over the slab surface.

Experimental program

Ordinary Portland cement was used to produce the concrete mix used in the present work. For all slabs, cast-in situ concrete was used and the designed mix consists of ingredients listed in Table 1 by weight.

Both of the main reinforcement and the DTS fixing processes upon the prepared molds were conducted first before concrete casting, as shown in Figure 4. Six cubes ($150 \times 150 \times 150$ mm) were used to perform compressive strength tests using a digital compressive machine with a maximum capacity of 2,000 kN with a loading rate of $0.9 \text{ kN}\cdot\text{s}^{-1}$ in accordance with the standard BS 8110-1 (British Standards Institution [BSI], 1997). All cubes were tested after 28 days curing and the average compressive strength value of six cubes was calculated producing $f_{cu} = 41.3 \text{ MPa}$ and $f_c = 33 \text{ MPa}$.

All slabs' models were tested, in the structural laboratory, using 2,000 kN capacity hydraulic machine (universal machine) under $5 \text{ kN}\cdot\text{min}^{-1}$ loading rate, to record the ultimate flexural load. Specimens of the RCOWS group were tested until failure under two-line load, as shown in Figure 5a.

The specimens were simply supported and the supports were placed at 100 mm from the ends of the slab's edges producing 1,800 mm clear span. For the RCTWS specimens, the slabs were neatly positioned on a steel frame that acted as basic supports on four sides, as shown in Figure 5b. The effective span was 950 mm in each direction and all four supports lines were positioned at 25 mm from the slab's edges. For all tests, the central deflections were measured using a dial gauge with a sensitivity of 0.01 mm per division. Crack emergence was carefully monitored, using the crack reader, in the first stage of loading to assign and record the load value corresponding to the first generated crack. This process was continued until the failure stage reaching. As the failure occurs, the load of failure was registered when the load becomes constant with an increase in deformation referring to the complete failure.

Results and discussion

Experimental test results for the RCOWS group

This group contains eight specimens of one-way slab models identified as SOC, SOLS, SOUS, SOUDH, SOUDV, SOUSO1,

TABLE 1. Components of the concrete mix

Average compressive strength after 28 days [MPa]	Cement content [$\text{kg}\cdot\text{m}^{-3}$]	Fine aggregate content [$\text{kg}\cdot\text{m}^{-3}$]	Coarse aggregate content [$\text{kg}\cdot\text{m}^{-3}$]	Water content [$\text{kg}\cdot\text{m}^{-3}$]
33	450	900	800	228



FIGURE 4. Reinforcement and DTS fixing processes and concrete casting for the RCOWS and RCTWS models



FIGURE 5. Locations of supports and point loads for (a) RCOWS models and (b) RCTWS models

SOUSO2 and SOUSO3, which were described earlier. During the test, each model was tested such that the load was gradually subjected until the first crack appears and the first crack load in the sagging zone (at mid span) was recorded. Then, as the applied load was increased, more cracks started to form and propagate in the tension zone until the complete failure which was a flexural failure mode for all of the tested specimens such as SOC and SOUS specimens shown in Figure 6.

For each specimen, the experimentally recorded first crack load and the ultimate load as well as the observed mode of failure are listed in Table 2. In Table 2, the last column represents the percentage of increasing in the ultimate load for each DTS reinforced specimen compared to the control specimen (SOC). It is observed that the ultimate increasing ratio was 80% for the case of Soudh specimen while the lower increasing ratio was 16% for the case of



FIGURE 6. SOC models (a) and SOUS models (b) in the complete failure

SOUSO3 specimen compared to the control specimen. The reason of better performance for the SOUDH specimen compared to SOUDV specimen could be attributed to the location of the two horizontally applied strips that are not interacted with the compression zone of the slab. This case happened in the case of SOUDV specimen which has DTS interacted through the slab compression zone that is not acted to enhance the flexural strength.

Figure 7 shows the load–deflection curves for all specimens investigated in the RCOWS group.

The behavior of all specimens was elastic following the same path until the first crack load. The first crack load was increased by

100% for all of the DTS – reinforced slabs compared to the control (SOC) specimen. In the second stage, the load–deflection curves behaved nonlinearly until the complete failure. In this stage, the failure was in flexural mode and it was noted that all specimens failed without any separation between the DTS and the surrounding concrete due to the efficient mechanism of shear connectors provided by the well distributed steel nails.

In case of overlapping the DTS, it was observed that the overlapping distance of 200 mm behaved better than other cases of 50 and 100 mm overlapping distances which produced an increase in load capacity of 70% relative to the control slab. Also, the use of double DTS layers placed horizontally

TABLE 2. Experimental test results for the RCOWS models

Specimen	DTS reinforcement	First crack load [kN]	Ultimate load [kN]	Increasing ratio [%]
SOC	no DTS reinforcement	5	25	–
SOLS	reinforced with single layer down	10	35	40
SOUS	reinforced with single layer up	10	33	32
SOUDH	reinforced with double layer horizontally	10	45	80
SOUDV	reinforced with double layer vertically	10	37	48
SOUSO1	reinforced with single overlap (100 mm)	10	30	20
SOUSO2	reinforced with single overlap (200 mm)	10	42.5	70
SOUSO3	reinforced with single overlap (50 mm)	10	29	16

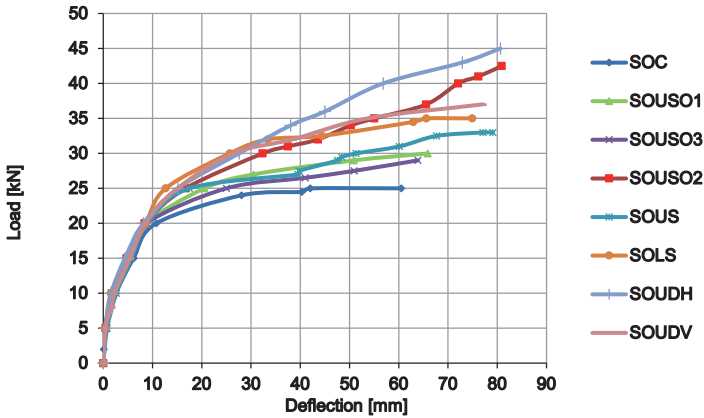


FIGURE 7. Load-deflection curves for the RCOWS group

enhance the ultimate load better than the case when the double strips placed vertically. Furthermore, the use of a single layer of DTS applied in the tension zone at zero elevation from the lower face of the model behaved better than the case when the DTS was applied at elevation of 25 mm from the lower face of the slab specimen. On the other hand, deflection values corresponding to each load value have decreased in the DTS – reinforced specimens compared to the control specimen showing a significant decrease in crack width for the DTS reinforced specimens.

Experimental test results for the RCTWS group

For both specimens adopted in the RCTWS group, identified as STC and STR, the applied load was subjected gradually until the first crack appearing. The cracks continued to appear in the tension face simultaneously with the load increasing until the complete failure of the specimen at ultimate load, as shown in Figure 8.

The test results of this specimen showed an increase in the first cracking load in the sagging zone and failure load of 100% and

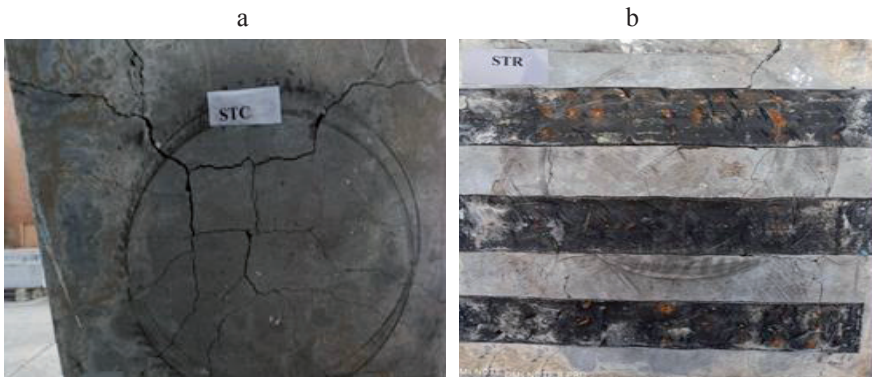


FIGURE 8. Lower face at complete failure of the (a) STC specimen and (b) STR specimen

14.286% respectively compared with the control slab STC, as listed in Table 3.

The ultimate load was increased (Table 3) with the decreasing in the deflection values when using the DTS as an additional reinforcement compared with the control specimen (Fig. 9). The amount of increasing value in ultimate load in this case study is relatively low compared with the RCOWS group cases of study due to the high stiffness of the RCTWS case study. Nevertheless, DTS was able to increase the ultimate load value which reflects the ability of adopting this material as an additional reinforcement in the structural element with relatively high stiffness property.

Statistical comparison

Due to the innovative approach of using DTS as an additional reinforcement in the reinforced concrete slabs proposed in the

present study, there is no similar study available in literature to do a comparison with the obtained results. However, a statistical comparison could be implemented with another and similar strengthening material represented by the carbon fiber reinforced polymer (CFRP) that used for the same purpose. Increasing the flexural load values due to the DTS were compared with the corresponding values when using CFRP for one-way slab models obtained by Omar and Rajai (2020) as well as the results of Rami, Jamal and Hasan (2016). On the other hand, results of the increasing in flexural load capacity of the two-way slab models obtained in the present study were compared with results obtained by Dina (2019), and Balamurugan and Viswanathan (2020), as listed in Table 4.

Taking into consideration the highly cost of the CFRP compared with the approximately free cost of the DTS, the use of DTS as a strengthening material provide a good

TABLE 3. Experimental test results for the RCTWS models

Specimen	DTS reinforcement	First crack load [kN]	Ultimate load [kN]	Increasing ratio [%]
STC	no DTS reinforcement	15	112	–
STR	reinforced with DTS strips	30	128	14.286

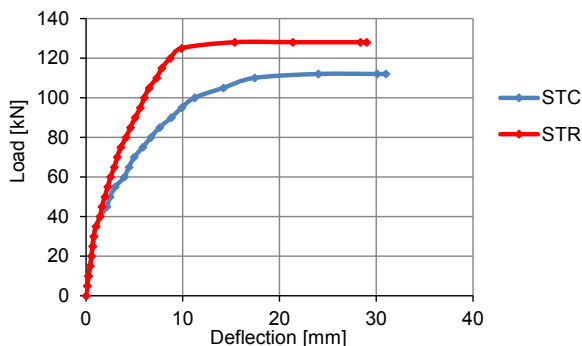


FIGURE 9. Load-deflection curves for the RCTWS group

TABLE 4. Increasing in the flexural load due to the DTS compared with the CFRP

Type of the slabs		Increasing ratios in the flexural load capacity [%]		
One-way slabs	reference	results of the present work using DTS	results of Omar and Rajai (2020) using CFRP	results of Rami et al. (2016) using CFRP
	min. ratio	16.00	41.80	69.00
	max. ratio	80.00	163.00	95.80
Two-way slabs	reference	results of the present work using DTS	results of Balamurugan and Viswanathan (2020) using CFRP	Results of Dina (2019) using CFRP
	min. ratio	–	19.45	72.00
	max. ratio	14.29	97.37	131.90

economically and friendly-environment option to enhance the flexural load capacity of the reinforced concrete slabs, as shown in Table 4.

Conclusions

In the present study, strips extracted from damaged vehicles tires were investigated experimentally as an innovative additional reinforcing material used for the reinforced concrete one-way slabs (RCOWS) and the reinforced concrete two-way slabs (RCTWS) models in addition to the main steel reinforcement to achieve the clean environment and economic considerations. The most significant observations obtained by this research could be stated as following:

- Damaged tires strips (DTS) behaved effectively as an additional reinforcing material for the reinforced concrete one-way slab (RCOWS) specimens that could increase the ultimate flexural load capacity within the range of 16–80%, depending on the case study. On the other hand, ultimate flexural load was increased for the reinforced concrete two-way slab (RCTWS) models of 14.286% for the DTS – reinforced specimen compared to the control specimen. The DTS could be

used within the reinforced concrete slabs with no separation between the DTS and the surrounding concrete due to the sufficient shear strength provided by the well distributed steel nails.

- In case of overlapping the DTS, present study recommends that the overlapping distance better to be at least 200 mm that increases load capacity by about 70% relative to control slab and the use of double DTS layers placed horizontally enhances the ultimate load better than the case when the double strips placed vertically. Also, the using of a single layer of DTS applied in the tension zone at zero elevation from the lower face of the model behaves better than the case when the DTS is applied at elevation of 25 mm from the lower face of the slab specimen.
- Using of the DTS in the reinforced concrete one-way and two-way slabs models increases the first crack load by 100% compared to the control specimens. On the other hand, deflection values corresponding to each load value have decreased in the DTS reinforced specimens compared to the control specimen showing a significant decrease in the crack width values for the DTS – reinforced specimens.

- Compared with the high cost of the CFRP, the use of DTS as a strengthening material provide a good economically and friendly-environment solution to enhance the flexural load capacity of the reinforced concrete one-way and two-way slabs.

References

- Balamurugan, G. & Viswanathan, T. S. (2020). Evaluation of the effects of orientation and coverage areas of FRP lamination bonded with two-way RC slabs – a modular approach. *Civil Engineering and Architecture*, 8 (4), 706–713.
- Bdour, A. N. & Al-Khalayleh, Y. A. (2010). Innovative application of scrap-tire steel cords in concrete mixes. *Jordan Journal of Civil Engineering*, 4 (1), 55–61.
- British Standards Institution [BSI] (1997). Structural use of concrete. Code of practice for design and construction (BS 8110-1). London: British Standards Institution.
- Bulei, C., Todor, M. P., Heput, T. & Kiss, I. (2018). Directions for material recovery of used tires and their use in the production of new products intended for the industry of civil construction and pavements. *Materials Science and Engineering*, 294 (1), 012064. <https://doi.org/10.1088/1757-899X/294/1/012064>
- Cao, W. (2007). Study on properties of recycled tire rubber modified asphalt mixtures using dry process. *Construction and Building Materials*, 21 (5), 1011–1015.
- Cecich, V., Gonzales, L., Hoisaeter, A., Williams, J. & Reddy, K. (1996). Use of shredded tires as lightweight backfill material for retaining structures. *Waste Management & Research*, 14 (5), 433–451.
- Celik, O. N. & Atiş, C. D. (2008). Compactibility of hot bituminous mixtures made with crumb rubber-modified binders. *Construction and Building Materials*, 22 (6), 1143–1147.
- Dina, A. E. (2019). Numerical study to investigate the behavior of reinforced concrete slabs with CFRP sheets. *Water Science*, 33 (1), 142–153.
- Edeskär, T. (2004). *Technical and environmental properties of tyre shreds focusing on ground engineering applications* (doctoral dissertation). University of Technology, Luleå.
- Edil, T. B., Park, J. K. & Kim, J. Y. (2004). Effectiveness of scrap tire chips as sorptive drainage material. *Journal of Environmental Engineering*, 130 (7), 828–831.
- Elnour, M. G. & Laz, H. A. (2014). Tire hazardous, disposal and recycling. *Journal of Applied and Industrial Sciences*, 2 (2), 63–74.
- Garrick, G. M. (2005). *Analysis and testing of waste tire fiber modified concrete* (master dissertation). Louisiana State University, Baton Rouge.
- Habib, A., Yildirim, U. & Eren, O. (2020). Mechanical and dynamic properties of high strength concrete with well graded coarse and fine tire rubber. *Construction and Building Materials*, 246, 118502. <https://doi.org/10.1016/j.conbuildmat.2020.118502>
- Li, L., Ruan, S. & Zeng, L. (2014). Mechanical properties and constitutive equations of concrete containing a low volume of tire rubber particles. *Construction and Building Materials*, 70, 291–308.
- Omar, A. & Rajai, Z. A. (2020). Response of reinforced concrete slabs strengthened with CFRP. *Journal of Engineering Science and Technology Review*, 13 (6), 125–129.
- Pilakoutas, K., Neocleous, K. & Tlemat, H. (2004). Reuse of tyre steel fibres as concrete reinforcement. *Proceedings of the Institution of Civil Engineers – Engineering Sustainability*, 157 (3), 131–138.
- Rami, H., Jamal, A. & Hasan, M. (2016). *Strengthening of thin reinforced concrete slabs with CFRP laminates*. 7th International Conference on Advanced Composite Materials in Bridges and Structures, 24–26 August 2016.
- Sengul, O. (2016). Mechanical behaviour of concretes containing waste steel fibers recovered from scrap tires. *Construction and Building Materials*, 122 (9), 649–658.
- Sharaky, I. A., Mohamed, H. A., Torres, L. & Emara, M. (2020). Flexural behavior of rubberized concrete beams strengthened in shear using welded wire mesh. *Composite Structures*, 247, 112485. <https://doi.org/10.1016/j.compstruct.2020.112485>

- Shu, X. & Huang, B. (2014). Recycling of waste tire rubber in asphalt and Portland cement concrete: An overview. *Construction and Building Materials*, 67, 217–224.
- Simalti, A. & Singh, A. P. (2021). Comparative study on performance of manufactured steel fiber and shredded tire recycled steel fiber reinforced self-consolidating concrete. *Construction and Building Materials*, 266 (1), 121102. <https://doi.org/10.1016/j.conbuildmat.2020.121102>
- Valente, M. & Sibai, A. (2019). Rubber/crete: Mechanical properties of scrap to reuse tire-derived rubber in concrete; A review. *Journal of Applied Biomaterials & Functional Materials*, 17 (1_suppl.), 2280800019835486. <https://doi.org/10.1177/2280800019835486>
- Yildirim, Y. (2007). Field performance comparison of asphalt crack-filling materials: hot pour versus cold pour. *Canadian Journal of Civil Engineering*, 34 (4), 505–512.

Summary

Enhancing the flexural load capacity of the reinforced concrete simply supported slabs using damaged tires strips (DTS). Damaged tires or ended-life tires

represent a difficult problem due to their ability to sustain for a long time which are not able to be dissolved easily. Present study focuses on the ability of using the damaged tires strips (DTS) in the field of structural engineering as an innovative reinforcing material used additionally with the main reinforcement. The adopted technique in the present work represents a clean solution to reuse and recycle DTS to increase the ultimate flexural capacity of the reinforced concrete one-way and two-way slabs used in structural systems satisfying clean environment and economic considerations. The tests were conducted upon eight specimens of reinforced concrete one-way slabs (RCOWS) and two specimens of reinforced concrete two-way slabs (RCTWS) reinforced by the DTS as an additional reinforcement. Experimentally obtained results exhibited enhancement for the ultimate flexural load capacity of the RCOWS and RCTWS models reinforced by the DTS in the range of 16–80 and 14.28% respectively, compared to the original reference specimens.

Eva VÍTKOVÁ   <https://orcid.org/0000-0002-2028-953X>

Lucie VAŇKOVÁ  <https://orcid.org/0000-0001-9440-8936>

Aneta OBLOUKOVÁ  <https://orcid.org/0000-0002-0630-3374>

Brno University of Technology, Faculty of Civil Engineering, Czech Republic

COMPARISON OF THE PRICE LEVEL OF THE WATER AND SEWERAGE CHARGE RATES AND MACROECONOMIC INDICATORS IN THE CZECH REPUBLIC

Key words: water and sewerage, charge rates, water supply and sewerage, gross domestic product, net household income

Introduction

Water supply and sewerage system operation is a public service that is supplied to the citizens of the state both in the Czech Republic and many other countries. As this is a public service, its price level should be acceptable to all citizens, in other words, the citizens should be able to pay for this public service. This article is focused on comparing the development of the price level of the water and sewerage charge rates in the regions of the Czech Republic to the

development of macroeconomic indicators expressing the performance of the individual region. The above raised to the research hypothesis of whether regions with lower performance also have a lower price level of water and sewerage charge rates from the point of view of the purchasing power of the inhabitants of this region. Tsur focused in his article on optimal water pricing, where he states that “A pricing-based mechanism that implements the optimal water policy while accounting for environmental externalities is developed” (2020, p. 1). Wait and Petrie (2017) conducted research into the comparison of water prices of public and private water companies in the United States. The relation between water utility ownership structure and water price was

researched in this study, along with other factors such as water source, population size, population density, population growth trends, service area size, and drought condition. In their article, Ashoori, Dzombak and Small (2017) dealt with the identification of water price and population criteria to meet future urban water demand targets. The research concluded that water demand in Los Angeles should increase by 36% between 2014 and 2050 and that future household water demand will be largely driven by the price and population rather than climate change and environment protection. The same approach applies to the price level of water and sewerage charge rates which represent the supply of public service in the sense of the water supply and sewerage system operation. Borhan, Ridzuan, Subramaniam, Amin and Saad (2021) addressed the relationship between polluted water and economic growth by using the environmental Kuznets curve analysis for the situation in Malaysia. In their study, they proposed how to focus on supporting investment in the appropriate technologies, especially sewerage systems and others.

The Czech Republic is not a very large country, it has about 10.5 million inhabitants. The state is divided into 14 regions and their performance varies. This performance is mainly related to the macroeconomic indicators, i.e. gross domestic product (GDP), unemployment rate and others. A number of authors have examined the differences in various macroeconomic aspects in the individual regions of the Czech Republic. For example, the relationship between tourism entities and economic performance expressed in terms of GDP was addressed by the research of Tuckova and Sverak (2016). The website www.czso.cz of the Czech Statistical Office (*Český statistický úřad*)

publishes the values of macroeconomic indicators of the Czech Republic, which are used for comparison with other countries, as well as macroeconomic indicators of individual regions, which can be used for regional comparison within the country. In their paper, Behun, Gavurova, Tkacova and Kotaskova (2018) worked with time series of selected macroeconomic indicators and monitored the dependence between the manufacturing industry and GDP, which represents the economic cycle in the European Union.

Zhukova and Sobolieva-Tereshchenko (2021) dealt with the method of analysing the dynamics of macroeconomic indicators in selected European countries in their article. The tool for predicting the indicators of the GDP type in 44 countries and three country aggregates is described separately in the article by Garnitz, Lehmann and Wohlrabe (2019). The website www.eagri.cz of the Ministry of Agriculture of the Czech Republic (*Ministerstvo zemědělství*) lists the price level of water and sewerage charge rates nationwide and also for individual regions. Since the 1990s, the water supply and sewerage operators transformed from state-owned enterprises into mostly joint-stock companies, i.e. capital companies that aim to satisfy their shareholders on dividends paid, so it is not always the case that the region with high performance has the highest water and sewerage charge rates. Therefore, the team of researchers focused both on the performance of the regions and the water management companies, which are water supply and sewerage system operators. Liu, Wu, Xu and Pan (2018) monitored the link between wastewater discharge, river water quality in the Pearl river delta and GDP per capita between 1999 and 2015. They used the logarithmic mean

division index decomposition model as well as the environmental Kuznets curve model for their research. Changes in the profit, productivity and price performance in the water and sewerage management industry within the empirical application for England and Wales were addressed by Maziotis, Saal, Thanassoulis and Molinos-Senante (2014). Their study analyses the impact of the regulation on the financial performance of water and sewerage companies in England and Wales in the period 1991–2008.

In another study, Molinos-Senante, Maziotis and Xue (2021) examined productivity growth, saving resulting from the scope and extent of the water and sewerage industry: the case study of Chile. In this article, they focused on performance evaluation and cost factor analysis of water companies, where they used quadratic cost functions to examine the existence of savings in the Chilean water and sewerage industry in the period 2010–2017. In their article, Frone and Frone (2014) dealt with the correlation between water supply and sewerage infrastructure and the economic development indicator GDP per capita at the regional county level. The article by Somlyódy and Patziger (2012) outlines the development of the technical infrastructure (water supply, sewerage and wastewater treatment) since 1990 in six countries, including the Czech Republic as well as influencing factors such as GDP, water charge rates, etc. The relationship between the industrial wastewater discharge and gross domestic product (GDP) per capita and urban domestic sewerage and GDP per capita is researched in his article by Liu (2019).

The presented article focuses on a part of the research, namely on presenting a com-

parison of the price level of the water and sewerage charge rates and macroeconomic indicators, which represent the performance of individual regions of the Czech Republic.

Material and methods

The Czech Republic consists of 14 regions: the Capital City of Prague, South Bohemian Region, South Moravian Region, Karlovy Vary Region, Vysočina Region, Hradec Králové Region, Liberec Region, Moravian-Silesian Region, Olomouc Region, Pardubice Region, Plzeň Region, Central Bohemia Region, Ústí nad Labem Region and Zlín Region (Fig. 1).

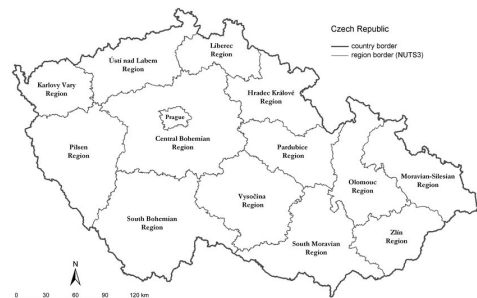


FIGURE 1. Regions of the Czech Republic (Kostin & Halounová, 2019)

The development, construction and operation of water supply and sewerage systems, which serve public needs, is addressed by the Water Supply and Sewerage Act of 2001 (274/2001 Coll.). Section 2 states that water supply and sewerage systems for public use are set up and operated in the public interest. For this reason, the following research hypothesis whether there is relation between regions and the price level of water and sewerage charge rates arose, i.e. that

“Do the regions with lower macroeconomic performance have lower price level of water and sewerage charge rates than the regions with higher macroeconomic performance?”.

Table 1 shows the price level of water and sewerage charge rates in individual regions of the Czech Republic for the last five years (the research is based on a 14-year period, 2007–2020).

Many authors deal with the influence of various factors on the efficiency in water management, respectively, in water and sewerage companies. For example, Molinos-Senante, Sala-Garrido and Lafuente (2015) addressed the impacts of environmental variables on the efficiency of water and sewerage companies: in a case study from Chile. The same authors also assessed the relative efficiency of water companies: a cross-border approach in the English and Welsh water industries, pointing to different services provided by water and sewerage companies as there are companies providing only water supply and the water

and sewerage companies (Molinos-Senante, Maziotis & Sala-Garrido, 2015).

The case study, which deals with the development of the level of water and sewerage charges and the development of macroeconomic indicators focuses on the regions in the Czech Republic. The case study examined 14 regions in the 2007–2020 period. One hundred ninety-six items of data were compared for the purposes of comparing the price level of water and sewerage charge rates. One thousand one hundred seventy-six items of data were compared within macroeconomic indicators and the following factors were monitored: population, gross domestic product at current prices, gross domestic product per capita, net disposable income of households, net disposable income per capita and average gross monthly wage per capita.

The comparison of the development of the price level of water and sewerage charge rates and macroeconomic indicators was created using a matrix expression.

TABLE 1. Development of the price level of the water and sewerage charge rates in CZK·m⁻³ in the regions of the Czech Republic in 2016–2020 (own processing based on data from eAGRI portal)

Item	2016	2017	2018	2019	2020
Capital City of Prague	72.40	74.40	76.00	78.00	84.00
Central Bohemia Region	70.30	72.70	74.00	76.10	81.70
South Bohemia Region	64.00	65.00	66.40	67.50	70.10
Plzeň region	64.20	65.10	67.00	71.30	75.40
Karlovy Vary Region	70.40	71.20	73.80	76.90	79.70
Ústí nad Labem Region	84.40	84.80	85.10	86.00	89.00
Liberec Region	84.10	84.90	86.70	87.70	90.00
Hradec Králové Region	67.30	67.80	69.10	71.70	74.60
Pardubice Region	66.60	68.00	70.30	73.20	76.00
Vysočina Region	61.70	63.90	65.40	67.30	70.30
South Moravian Region	66.70	67.10	69.00	72.30	76.60
Olomouc Region	63.10	63.80	65.20	68.00	71.30
Zlín Region	65.20	65.60	66.60	69.20	71.70
Moravian-Silesian Region	63.80	65.00	65.90	69.10	72.60

Note: 1 EUR = 25.50 CZK.

The partial matrix expression, separately for the price level of the water and sewage charge rates and macroeconomic indicators, is two-dimensional, where 14 rows and single column were specified, $\mathbf{A} = (a_{ij})$.

$$\mathbf{A} = \begin{pmatrix} a_{11} \\ a_{21} \\ \vdots \\ a_{m1} \end{pmatrix}, \quad (1)$$

where:
 $m = 14$.

Fourteen two-dimensional matrices were created for the price level of water and sewage charge rates, i.e. matrices \mathbf{A} – \mathbf{N} , from which the \mathbf{AA} matrix was subsequently created.

$$\mathbf{AA} = \begin{pmatrix} a_{11} & a_{12} & a_{1n} \\ a_{21} & a_{22} & a_{2n} \\ \vdots & \vdots & \vdots \\ a_{m1} & a_{m2} & a_{mn} \end{pmatrix}, \quad (2)$$

where:
 $m = 14$,
 $n = 14$.

Seventy two-dimensional matrices were created for the macroeconomic indicators, i.e. the \mathbf{A}' – \mathbf{SSS}' matrix, from which the \mathbf{BB} matrix was created.

$$\mathbf{BB} = \begin{pmatrix} b_{11} & b_{12} & b_{1n} \\ b_{21} & b_{22} & b_{2n} \\ \vdots & \vdots & \vdots \\ b_{m1} & b_{m2} & b_{mn} \end{pmatrix}, \quad (3)$$

where:
 $m = 14$,
 $n = 14$.

The final \mathbf{AAA} matrix for the price level of the water and sewerage charge rates is based on the sum of the matrices \mathbf{A} – \mathbf{N} .

$$\mathbf{AAA} = \mathbf{A} + \mathbf{B} + \mathbf{C} + \mathbf{D} + \dots + \mathbf{N}, \quad (4)$$

$$\mathbf{AAA}_{ij} = \mathbf{A}_{ij} + \mathbf{B}_{ij} + \mathbf{C}_{ij} + \mathbf{D}_{ij} + \dots + \mathbf{N}_{ij}. \quad (5)$$

The final \mathbf{BBB} matrix for the macroeconomic indicators is based on the sum of matrices \mathbf{A}' – \mathbf{SSS}' .

$$\mathbf{BBB} = \mathbf{A}' + \mathbf{B}' + \mathbf{C}' + \mathbf{D}' + \dots + \mathbf{SSS}', \quad (6)$$

$$\mathbf{BBB}_{ij} = \mathbf{A}'_{ij} + \mathbf{B}'_{ij} + \mathbf{C}'_{ij} + \mathbf{D}'_{ij} + \dots + \mathbf{SSS}'_{ij}. \quad (7)$$

The output matrix, which combines the outputs of the matrix expressions of the price level of water and sewerage charge rates (a) and the matrix expressions of macroeconomic indicators (b), has the following form:

$$\mathbf{AB} = \begin{pmatrix} a_{11} & b_{12} & b_{1n} \\ a_{12} & b_{22} & b_{2n} \\ \vdots & \vdots & \vdots \\ a_{m1} & b_{m2} & b_{mn} \end{pmatrix}, \quad (8)$$

where:
 $m = 14$,
 $n = 7$.

Results and discussion

As already mentioned in the introduction to this article, water supply and sewerage management in the Czech Republic is regulated by the Water Supply and Sewerage Act of 2001. This law clearly defines that water supply and sewerage systems for public use are established and operated in the public interest. This statement can be understood as a public service. The Czech Republic has about 10.5 million inhabitants, for whom it is necessary to supply water and discharge sewerage. The Czech Republic is divided into 14 regions, which are diverse in terms of both performance and economic efficiency. The Capital City of Prague is one of the regions with the highest performance which always influences all national statistics by its above-standard values.

Based on the collection of data on the price level of the water and sewerage charge rates in individual regions of the Czech Republic, their analysis in the monitored years 2007–2020 where the order was determined for each year (1–the lowest price, 14–the highest price) and the matrix expression created, a two-dimensional Table 2 was compiled.

TABLE 2. The final order for the monitored years 2007–2020 for the price level of water and sewerage charge rates in the regions of the Czech Republic (own processing)

Description	Point evaluation	Final order
Vysočina Region	31	1
Olomouc Region	41	2
Plzeň Region	47	3
Moravian-Silesian Region	47	4
South Bohemian Region	81	5
South Moravian Region	96	6
Zlín Region	98	7
Hradec Králové Region	102	8
Pardubice Region	111	9
Central Bohemian Region	144	10
Capital City of Prague	147	11
Karlovy Vary Region	147	12
Liberec Region	187	13
Ústí nad Labem Region	190	14

Based on the data collection on the following macroeconomic indicators:

- gross domestic product (GDP),
- gross domestic product per capita (GDP per capita),
- net disposable income of households (NDI),
- net disposable income of households per capita (NDI per capita),
- average gross wage,

in individual regions of the Czech Republic, their analysis in the monitored years

2007–2020, where the following order was determined for each year:

- gross domestic product: 1 – the highest value, 14 – the lowest value,
- gross domestic product per capita: 1 – the highest value, 14 – the lowest value,
- net disposable income of households: 1 – the highest value, 14 – the lowest value,
- net disposable income of households per capita: 1 – the highest value, 14 – the lowest value,
- average gross wage: 1 – the highest value, 14 – the lowest value,

a matrix expression was performed from the following outputs (Table 3).

Table 4 combines output data related to the price level of water and sewerage charges and individual macroeconomic indicators in the regions of the Czech Republic. This output table contains data that answers the basic research question stated in the introductory part of this article: whether regions with lower performance have a lower price level of water and sewage charge rates if this service to the population is considered to be a public service by law.

The Plzeň Region is not one of the regions with the lowest performance in terms of macroeconomic indicators. On the other hand, the Plzeň Region is one of the most efficient regions in terms of gross domestic product per capita, net disposable income of households per capita and net disposable income of household performances. An overview of the order for the level of water and sewerage charges and individual macroeconomic indicators is shown in Table 5, which shows the sum of individual matrix expressions within macroeconomic indicators and shows two dimensions: namely the order of the level of the water

TABLE 3. The final order for the monitored years 2007–2020 within individual macroeconomic indicators in the regions of the Czech Republic (own processing)

Description	GDP	GDP per capita	NDI	NDI per capita	Average gross wage
Capital City of Prague	1	1	1	1	1
Central Bohemia Region	2	4	2	2	2
South Bohemia Region	6	7	6	7	7
Plzeň Region	7	3	8	3	3
Karlovy Vary Region	14	14	14	13	13
Ústí nad Labem Region	5	12	5	14	14
Liberec Region	13	11	13	10	10
Hradec Králové Region	10	5	10	5	5
Pardubice Region	12	10	12	8	8
Vysočina Region	11	9	11	6	6
South Moravian Region	3	2	3	4	4
Olomouc Region	9	13	7	12	12
Zlín Region	8	6	9	9	9
Moravian-Silesian Region	4	8	4	11	11

TABLE 4. The final order for the monitored years 2007–2020 for the price level of the water and sewerage charge rates and macroeconomic indicators in the regions of the Czech Republic (own processing)

Description	W/S	GDP	GDP per capita	NDI	NDI per capita	Average gross wage
Capital City of Prague	11	1	1	1	1	1
Central Bohemia Region	10	2	4	2	2	2
South Bohemia Region	5	6	7	6	7	7
Plzeň Region	3	7	3	8	3	3
Karlovy Vary Region	12	14	14	14	13	13
Ústí nad Labem Region	14	5	12	5	14	14
Liberec Region	13	13	11	13	10	10
Hradec Králové Region	8	10	5	10	5	5
Pardubice Region	9	12	10	12	8	8
Vysočina Region	1	11	9	11	6	6
South Moravian Region	6	3	2	3	4	4
Olomouc Region	2	9	13	7	12	12
Zlín Region	7	8	6	9	9	9
Moravian-Silesian Region	4	4	8	4	11	11

and sewerage charges and the sum of the order of macroeconomic indicators. They are always sorted from the lowest to the highest values.

Conclusions

The research focused on the basic research question “Do the regions with lower macroeconomic performance have a lower price level of water and sewerage charge rates than the regions with higher macroeconomic performance?”. Values from the timeline were taken for the research, namely from the years 2007–2020.

Thus, the researchers worked with 1,176 items of data on macroeconomic indicators and 196 items of data on the price level of the water and sewerage charge rates. Macroeconomic indicators focused on

the performance of the region, which was represented by gross domestic product, gross domestic product per capita, net disposable income of households, net disposable income of households per capita and average gross wage.

The research shows that the lowest price level of water and sewerage charge rates was in the Vysočina, Olomouc, Plzeň and Moravian-Silesian Regions (Table 2). On the contrary, the highest level of the water and sewerage charges was in the Karlovy Vary, Liberec and Ústí nad Labem Regions. Further from the research shows that the Karlovy Vary, Liberec and Olomouc Regions are among the regions with the lowest performance, while the Capital City of Prague, Central Bohemia and South Moravia Regions range among those with the highest performance (Table 5). It is clear from the above-stated facts that the research question

TABLE 5. The order of the price level of water and sewerage charge rates and the sum of macroeconomic indicators in the regions of the Czech Republic (own processing)

Order of the price level of the water and sewerage charge rates in the regions	Order of the sum of the macroeconomic indicators in the regions
Vysočina Region	Karlovy Vary Region
Olomouc Region	Liberec Region
Plzeň Region	Olomouc Region
Moravian-Silesian Region	Ústí nad Labem
South Bohemian Region	Pardubice Region
South Moravian Region	Vysočina Region
Zlín Region	Zlín Region
Hradec Králové Region	Moravian-Silesian Region
Pardubice Region	Hradec Králové Region
Central Bohemia Region	South Bohemia Region
Capital City of Prague	Plzeň Region
Karlovy Vary Region	South Moravian Region
Liberec Region	Central Bohemian Region
Ústí nad Labem Region	Capital City of Prague

has not been confirmed as only one region out of 14 meets this condition, namely the Olomouc Region. The research found that the difference in the price level of the water and sewerage charge rates with the lowest level in the Vysočina Region and the highest level in the Ústí nad Labem Region is on average 31.94% for the observed years 2007–2020. Similarly, the average percentage differences in macroeconomic indicators between the Capital City of Prague and the Karlovy Vary Regions were determined, namely:

- gross domestic product differs on average by 1,291.6%,
- gross domestic product per capita differs on average by 230.5%,
- net disposable income of households differs on average by 534.4%,
- net disposable income of households per capita differs on average by 50.5%,
- the average gross wage differs on average by 48.8%.

It is clear from the above-listed information that the equality between the price level of water and sewerage charge rates and macroeconomic indicators in the regions of the Czech Republic is not apparent. Further research will focus on determining the correlations between the price level of the water and sewerage charge rates, individual macroeconomic indicators and other technical indicators related to the water supply and sewerage systems operation, such as the length of the connections or the number of customers.

Acknowledgements

This paper has been worked out under the project of the junior specific research at the Brno University of Technology FAST-J-22-8030 “Development of the price of

water and sewage in the Czech Republic and individual regions, including macroeconomic indicators”.

References

- Ashoori, N., Dzombak, D. A. & Small, M. J. (2017). Identifying water price and population criteria for meeting future urban water demand targets. *Journal of Hydrology*, 555, 547–556. <https://doi.org/10.1016/j.jhydrol.2017.10.047>
- Behun, M., Gavurova, B., Tkacova, A. & Kotaskova, A. (2018). The impact of the manufacturing industry on the economic cycle of European Union countries. *Journal of competitiveness*, 10 (1), 23–39. <https://doi.org/10.7441/joc.2018.01.02>
- Borhan, H., Ridzuan, A. R., Subramaniam, G., Amin, S. M. & Saad, R. M. (2021). Modelling the environmental kuznets curve of water pollution impact on economic growth in developing country. *International Journal of Energy Economics and Policy*, 11 (5), 545–552. <https://doi.org/10.32479/ijeep.11571>
- Český statistický úřad (2020-03-28). Retrieved from: <https://www.czso.cz>
- Frone, S. & Frone, D. F. (2014). Challenges in analyzing correlation between water infrastructure and economic development. *Procedia Economics and Finance*, 10, 197–206. [https://doi.org/10.1016/S2212-5671\(14\)00294-9](https://doi.org/10.1016/S2212-5671(14)00294-9)
- Garnitz, J., Lehmann, R. & Wohlrabe, K. (2019). Forecasting GDP all over the world using leading indicators based on comprehensive survey data. *Applied Economics*, 51 (54), 5802–5816. <https://doi.org/10.1080/00036846.2019.1624915>
- Kostin, V. & Halounová, L. (2019). An analysis of spatial structure of urban regional networks using GIS. *Acta Polytechnica*, 59 (1), 35–41. <https://doi.org/10.14311/AP.2019.59.0035>
- Liu, J. (2019). Relationship between water pollution and regional economic development: Empirical evidence from Hubei, China. *Nature Environment and Pollution Technology*, 18 (2), 599–603.

- Liu, L., Wu, T., Xu, Z. & Pan, X. (2018). The water-economy nexus and sustainable transition of the Pearl River Delta, China (1999–2015). *Sustainability*, 10 (8), 2595. <https://doi.org/10.3390/su10082595>
- Maziotis, A., Saal, D. S., Thanassoulis, E. & Molinos-Senante, M. (2015). Profit, productivity and price performance changes in the water and sewerage industry: an empirical application for England and Wales. *Clean Technologies and Environmental Policy*, 17 (4), 1005–1018. <https://doi.org/10.1007/s10098-014-0852-2>
- Ministerstvo zemědělství (2020-03-28). eAGRI. Retrieved from: <https://www.eagri.cz>
- Molinos-Senante, M., Maziotis, A. & Sala-Garrido, R. (2015). Assessing the relative efficiency of water companies in the English and Welsh water industry: a metafrontier approach. *Environmental Science and Pollution Research*, 22 (21), 16987–16996. <https://doi.org/10.1007/s11356-015-4804-0>
- Molinos-Senante, M., Maziotis, A. & Xue, B. (2021). Productivity growth, economies of scale and scope in the water and sewerage industry: The Chilean case. *PLoS ONE*, 16 (5). <https://doi.org/10.1371/journal.pone.0251874>
- Molinos-Senante, M., Sala-Garrido, R. & Lafuente, M. (2015). The role of environmental variables on the efficiency of water and sewerage companies: a case study of Chile. *Environmental Science and Pollution Research*, 22 (13), 10242–10253. <https://doi.org/10.1007/s11356-015-4225-0>
- Somlyódy, L. & Patziger, M. (2012). Urban wastewater development in Central and Eastern Europe. *Water Science and Technology*, 66 (5), 1081–1087. <https://doi.org/10.2166/wst.2012.289>
- Tsur, Y. (2020). Optimal water pricing: Accounting for environmental externalities. *Ecological Economics*, 170, 106429. <https://doi.org/10.1016/j.ecolecon.2019.106429>
- Tuckova, Z. & Sverak, P. (2016). Impact of the regional macroeconomics indicators on tourism entities in Plzen and Zlin Regions. *Procedia Economics and Finance*, 39, 313–318. [https://doi.org/10.1016/S2212-5671\(16\)30329-X](https://doi.org/10.1016/S2212-5671(16)30329-X)
- Wait, I. W. & Petrie, W. A. (2017). Comparison of water pricing for publicly and privately owned water utilities in the United States. *Water International*, 42 (8), 967–980. <https://doi.org/10.1080/02508060.2017.140678e>
- Zákon o vodovodech a kanalizacích pro veřejnou potřebu a o změně některých zákonů (zákon o vodovodech a kanalizacích). Zákon č. 274/2001 Sb. [Act 274/2001 on water supply and sewerage for public use and on amendments to certain acts (Water Supply and Sewerage Act) on water supply and sewerage. Act No 274/2001 Coll.].
- Zhukova, Y. & Sobolievá-Tereshchenko, O. (2021). Modeling macroeconomic indicators in unstable economies. *Journal of International Studies (Kyiv)*, 14 (2), 128–148. <https://doi.org/10.14254/2071-8330.2021/14-2/9>

Summary

Comparison of the price level of the water and sewerage charge rates and macroeconomic indicators in the Czech Republic. This article focused on comparing the development of the price level of the water and sewerage charge rates in the regions of the Czech Republic to the development of macroeconomic indicators expressing the performance of the individual region. The following were selected as macroeconomic indicators: gross domestic product, gross domestic product per capita, net disposable income of households, net disposable income of households per capita and average gross wage. The Czech Republic is divided into 14 regions. In each region, a different price level of the water and sewerage charge rate was determined. At the same time, each region had a different performance which is represented by the above-mentioned macroeconomic indicators. The regions with the lowest performance are the Karlovy Vary, Liberec and Olomouc Regions. It follows from the definition of Act 274/2001 Coll. on the water supply and sewerage systems operation is in the public interest. This raised

the research hypothesis of whether regions with lower performance also have a lower price level of water and sewerage charge rates from the point of view of the purchasing power of the inhabitants of this region. Confirmation or rejection of this hypothesis was based on the creation of matrix expressions, in total 91 matrices. The input data for the creation of matrices contained

196 items of data on the price level of the water and sewerage charge rates and 1,176 items of data on macroeconomic indicators. The hypothesis was not confirmed as only one region met the condition (Olomouc Region), which had a lower price level of water and sewerage charge rates and lower efficiency.

Wan Farahiyah WAN KAMARUDIN¹✉

Zildawarni IRWAN¹

Mohd Rabani YAAFAR²

Abd Rahman MAT AMIN¹

¹Universiti Teknologi MARA, Faculty of Applied Science, Terengganu, Malaysia

²Universiti Teknologi MARA, Faculty of Applied Science, Perak, Malaysia

LOCKDOWN EFFECT ON CARBON MONOXIDE CONCENTRATION OVER MALAYSIA AND INDONESIA

Key words: carbon monoxide (CO), COVID-19, lockdown, pandemic, MERRA-2, Giovanni 4

Introduction

Coronavirus disease 2019, which is known as COVID-19, is a highly spreadable disease which was first discovered around December 2019 in Wuhan City, Hubei province, China. On 11 March 2020, the World Health Organization (WHO) had announced COVID-19 as a global pandemic as the novel coronavirus continues to spread worldwide extremely fast. Globally, up to 24 April 2021, there had been 145,216,414 confirmed cases and 3,079,390 deaths reported (World Health Organization [WHO], 2021). Malaysia, Indonesia

and other southeast Asian countries had enforced lockdown at different degrees to control the spread of the disease as did many other countries around the world too. Almost all mass transportation, economic activities and social activities were prohibited by this nationwide lockdown policies as many countries had been forced to keep their citizens safe at home. Owing to the movement limitation, there had been less vehicles on the roads, many cancelled flights and restricted industrial activities which led to decreasing levels of air pollutants in the environment. As a result of this lockdown effect, there has been a benefit on human health upon reduced air pollution.

Carbon monoxide (CO) is one of the air pollutants that needs to be monitored at

high resolution since these compounds will deteriorate human health if present at high concentrations (Manisalidis, Stavropoulou, Stavropoulos & Bezirtzoglou, 2020). Carbon monoxide is identified as chemically reactive trace gas that will threaten human health because it has 200 times greater affinity for hemoglobin than carbon dioxide (CO₂) (Perutz, 1990). Breathing high concentrations of CO leads to the reduced amount of oxygen transported in the blood stream to important human organs that can cause headaches, confusion, unconsciousness, brain damage or death (Fisher, Iscoe, Fedorko & Duffin, 2011). Carbon monoxide gas usually comes from four major sources: fossil fuel combustion, industrial combustion, biomass burning and oxidation of methane and other hydrocarbons (Azhari, Mohamed & Latif, 2016). Transportation combustion accounts about 50% of the total industrial source of carbon monoxide especially in the urban industrial areas (Azhari et al., 2016).

Globally, recent research has been focusing on the effect of the lockdown due to the COVID-19 pandemic on air quality especially on CO gas across nationwide. Collivignarelli et al. (2021) demonstrated a significant decrease of CO concentration mainly due to the severe limitation of people movements in the Metropolitan City of Milan following the partial and the subsequent total lockdown. Furthermore, Kerimray et al. (2020) in their study also proved that there was a significant decrease in CO concentrations by 49% during the COVID-19 lockdown period in Almaty, Kazakhstan compared to the days before the lockdown. The results could be due to the combination of seasonal weather changes and traffic elimination in Almaty, Kazakhstan. It may have also been considerably contributed by various non-traffic related

sources such as power plants and coal-fired combined heat. The effect of COVID-19 pandemic lockdown on the megacity Delhi, India air quality has also been investigated. The CO concentrations were monitored for different monitoring stations and the results proved that during lockdown it decreased and was indeed better compared to the time before lockdown. Moreover a research by Mahato, Pal and Ghosh (2020) found that CO concentration in the transportation and industrial area showed a significant decrease of 30.35% during lockdown phase. It is also reported that the decreasing trend of CO concentration was found on the second to fourth day of lockdown (Mahato et al., 2020).

There are several studies conducted on the lockdown impact due to the COVID-19 pandemic on Southeast Asian region on CO concentration especially in Malaysia and Indonesia. Nadzir et al. (2020) showed the effect of total lockdown in Klang Valley, Malaysia on CO gas during COVID-19 pandemic. From the observation, 48.7% of CO gas has been depleted. The results from this research revealed that the air pollutants such as CO gas could be reduced if the Malaysian authorities control the traffic and industry emissions strictly. In Jakarta, Indonesia, it was Anugerah, Muttaqin and Purnama (2020) who first conducted a study that used ground-level measurement data to measure the effect of lockdown on outdoor air quality. During lockdown, the CO concentration showed the most significant reduction at the percentage of 39.9% (Anugerah et al., 2020). Recent studies in Malaysia and Indonesia have only focused on big cities of these two countries and do not cover the entire country. Therefore, the focus of this paper is to determine the CO distribution over Malaysia and its neighbouring territory,

Indonesia, for a period from January 2011 to December 2021 using online Geospatial Interactive Online Visualization and Analysis Infrastructure (Giovanni). NASA Modern-Era Retrospective Analysis for Research and Applications, Version 2 (MERRA-2) provides the data for surface concentration of CO that has been used in this study. It is hoped that results from this study could assist the authorities in formulating the best management procedure and air quality control methods to control air pollution. This study is conducted to investigate a span of nine years of CO concentration over Malaysia and Indonesia.

Methodology

In this study, atmospheric dataset was obtained from the Giovanni 4 interface. Firstly, CO concentration analysis assimilated by Modern-Era Retrospective Analysis for Research and Applications, Version 2 (MERRA-2) was chosen. MERRA-2 is a NASA atmospheric reanalysis that provides data beginning in 1980 and known as the first long-term global reanalysis to provide an ongoing near-real-time climate analysis. It is intended as an intermediate reanalysis, developing an integrated Earth system analysis (IESA) capability that couples with the assimilation systems for the atmosphere, ocean, land, and chemistry. MERRA-2 also includes aerosol data assimilation, thereby providing a multidecadal reanalysis in which aerosol and meteorological observations are jointly assimilated within a global data assimilation system (Gelaro et al., 2017).

All data collections from MERRA-2 are provided on the same horizontal grid where this grid has 576 points in the longitudinal direction and 361 points in the latitudinal

direction, corresponding to a resolution of $0.625^{\circ} \times 0.5^{\circ}$ (Gelaro et al., 2017). After the study area was selected, the time averaged map for the period of January 2011 to December 2021 was plotted. The month-long lockdown is then constructed by using the same geographical coordinates. The month-long lockdown compute averages for January 2021 until December 2022 where mostly government around the world began nationwide lockdown. Time series were then plotted by using monthly area averaged time series that can be downloaded in Microsoft Excel format.

Study area

Geographically, Malaysia and Indonesia are located in Southeast Asia region (94.0869E, 9.4189S, 119.3994E and 7.4561N). It is bordered by the South China Sea to the east and Indian Ocean to the west. Malaysia is situated in central Southeast Asia, bordering in the north, with Singapore to the south and Indonesian to the south and west. Malaysia consists of Peninsular Malaysia and the states of Sabah and Sarawak on the north coast of the island of Borneo across the



FIGURE 1. The geographically feature of study area

South China Sea. Topographically, Indonesia is divided into three major regions: Sumatera to the north, Kalimantan to the east and Java to the south (Fig. 1).

Result and discussion

A spatial CO concentration is observed over the studied region. Figure 2 is a time averaged map that was constructed to find the general view of CO distribution over the study region (Malaysia and Indonesia). From the period of January 2011 to December 2021, there are five main regions that recorded high reading of CO concentration: Kuala Lumpur, Riau, Jambi, Palembang and Jakarta.

From this 10 years' time series, the highest spike was observed in Jakarta region that located at the south of island of Sumatera. The contributing factor for these high values of CO concentration is consistent with Rana, Mahmood, Tariq and Qayyum (2015) who reported that the increasing CO emission is

due to deforestation and urbanization in the region. The study conducted by Lavorel, Flannigan, Lambin and Scholes (2007) found that fire is a dominant factor that contributes to the largest anthropogenic influences CO emission after agricultural activities and urbanization. This is a very critical element that gives huge impacts to social, economic, and environmental activities. In addition, Southeast Asia has many social, economic, and environmental impacts caused by forest and land fires. Fire is considered one of the largest anthropogenic influences on terrestrial ecosystems after agricultural activities and urban, and it is indeed a critical element (Lavorel et al., 2007).

To find the exact time (year and month) that recorded the highest spike of CO concentration, area averaged time series for study period was constructed as shown in Figure 3. In this section, the 10-years of CO concentration retrieved over Jakarta, Kuala Lumpur, Riau, Palembang, and Jambi will be discussed.



FIGURE 2. Time averaged map of CO surface concentration in ppbv (ENSEMBLE) monthly $0.5^\circ \times 0.625^\circ$ over the period of January 2011 to December 2021

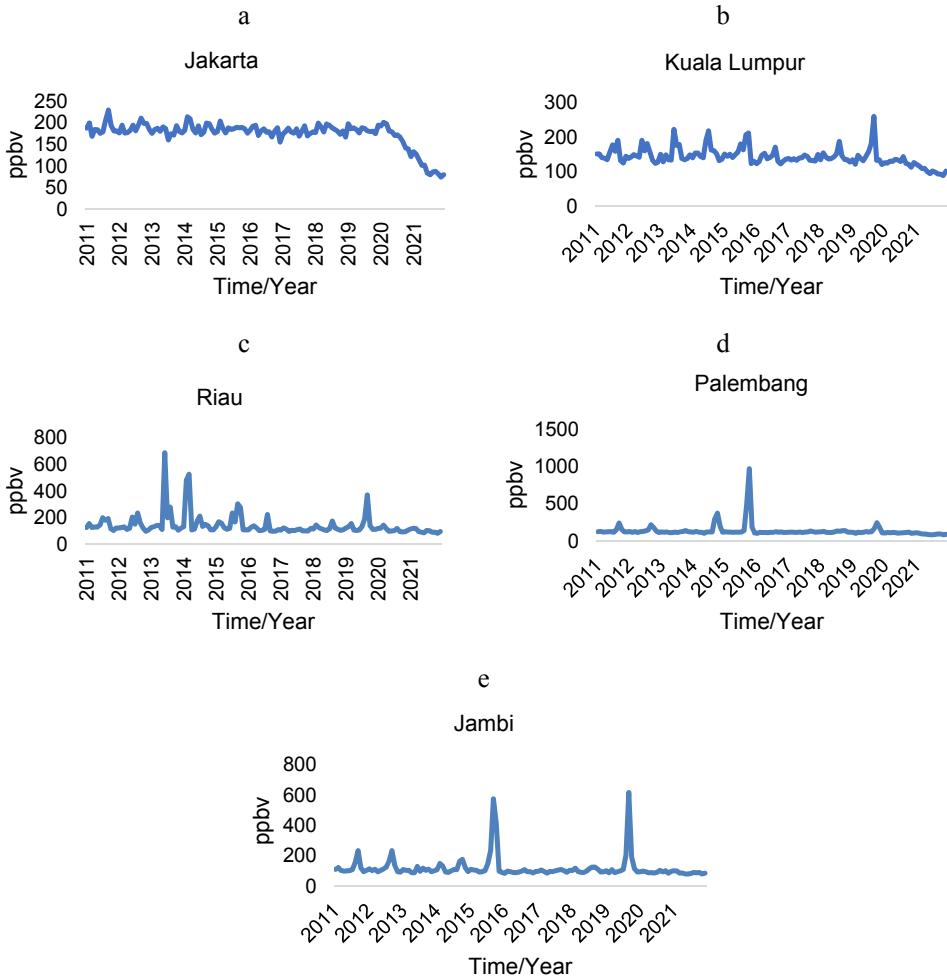


FIGURE 3. Area-averaged of CO surface concentration in ppbv (ESEMBLE) time series over (a) Jakarta, (b) Kuala Lumpur, (c) Riau, (d) Palembang, (e) Jambi from January 2011 to December 2021

Jambi and Riau region were reported as the worst region affected by the CO value as high as 638.4248 ppbv in June 2013, and Jambi was found with a CO concentration of 640.0425 ppbv in September 2019. The area averaged of CO concentration time series over Jakarta during the study period is presented in Figure 3a. For Jakarta, the satellite data show the highest spike in September 2011 and July 2018 with the

values of 372.353 ppbv and 372.0188 ppbv respectively. The highest spike recorded by Kuala Lumpur is 333.2772 ppbv in September 2019 as shown in Figure 3b.

Figure 3c presents the CO values over Riau region with four peaks exceeding 300 ppbv with increasing values of CO that were observed in June 2013, February to March 2014 and September 2019. The CO concentration over Palembang region

as shown in Figure 3d, observed the highest CO concentration with the value of 618.4915 ppbv in October 2015, followed by September 2019 with 314.7835 ppbv. As shown in Figure 3e, Jambi region was the most affected region during Indonesia's forest fire in September 2019; it exhibited the highest spike with the value of 640.0425 ppbv in September 2019 and 573.931 ppbv in September 2015.

The above findings show that the period with the high reading of CO concentration for the last 10 years is in September 2019. Studies conducted by Kamarudin, Muhammad, Sa'ad and Mustapha (2019) and Rajab, Tan, Lim and Mat Jafri (2019) discovered that the increasing CO concentration was mainly attributed to forest burning activities over Indonesia, automobiles, industrial activities, electricity generation, biomass and crop residue burnings that have caused adverse health and economic impacts not only to Malaysia and Indonesia, but also to Brunei Darussalam, Singapore and, to a lesser degree, the Philippines and Thailand. This is in line with an article reported by BBC Asia News (BBC, 2019) that stated the forest fire in

Indonesia had burnt 328,724 ha of land from January to August 2019. It also reported that large agricultural waste burning emission usually occurs from July to October during continuous dry season in Indonesia.

In order to trigger the exact location that had been most impacted by Indonesia forest fire in September 2019, a monthly area averaged was constructed as shown in Figure 4. It is observed that a high value of CO concentration exists over Jambi region which is associated with CO transport due to the occurrence of forest fire in central Sumatera's Jambi province. This is a combined effect causing the thick chocky haze that blanketed a large part of the region in September 2019 as reported by Kiki (2019). Freedman (2019) asserts that the wildfires turned the skies over Indonesia's Jambi province a dark blood red. This extreme biomass burning in Jambi, Indonesia in September 2019 had caused Malaysia and Indonesia to experience a high CO concentration which was significantly influenced by CO transport from the Jambi province.

As COVID-19 pandemic hit the whole world at the end of 2019, these five cities exhibited low level of CO concentration

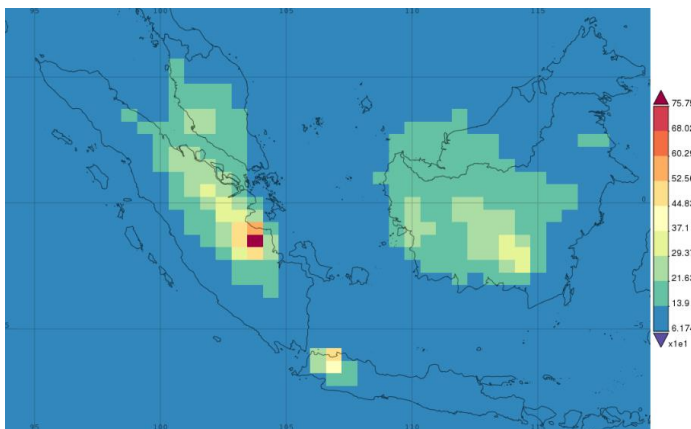


FIGURE 4. Monthly area averaged for September 2019

throughout 2020 and 2021. This is due to COVID-19 pandemic and most governments around the world began or extended nationwide lockdown to stem the coronavirus pandemic (Harris, 2020). It can be seen in Figure 5 where the comparison between CO concentration before COVID-19 pandemic (2019) and during COVID-19 pandemic (2020 and 2021) shows a decreasing trend from September 2019 to December 2021. In addition, from Figure 5, it seems likely that no high peak was recorded during dry season (July to October) in 2020 and 2021. As shown in Figure 5a, the CO concentration for Kuala Lumpur region was decreased after September 2019 and readings continued to decline in the year 2020 and 2021.

A responsible factor for this declining trends is the Movement Control Order (MCO) implemented by the federal government of Malaysia on 18 March 2020 as a preventive measure in response to COVID-19 pandemic. This restriction covers prohibitions on mass movement and gatherings countrywide, interstate, and inter-district travel bans among Malaysians, as well as entry and movement restrictions for the tourists. Government also issued “stay-at-home” order instructing residents to restrict their daily movements. Malaysia moved into the Conditional Movement Control Orders (CMCO) from 4 May 2020 and it ran until 9 June 2020. The CO concentration in August 2020 slightly increased higher as Malaysia moved into the Recovery Movement Control Order (RMCO) starting from 10 June until 31 December 2020 and then extended until 31 March 2021. As Malaysia was battling for the second wave of coronavirus spread, the total lockdown was implemented again from 1 June 2021 until 28 June 2021, which

then moved to the National Recovery Plan (NRP) from 15 June 2021 until 31 December 2021.

When MCO, CMCO, RMCO and NRP were implemented, the satellite data shows the decreasing trend of CO concentration compared to before the implementation of the series of lockdowns. This is in line with an article by Taufik (2020) who analysed the contrast pattern of lower CO concentration and fewer fire hotspots across the study region. He estimated that 206,751 ha of land area were affected by fire from January to September 2020 (during pandemic COVID-19). This author also found that the dry season in the year 2020 which was wetter than usual was responsible for the lower CO emission in the widespread smoke from the fire set by agricultural burnings in Sumatera and Kalimantan.

Meanwhile, starting from October 2019, the Indonesia regions of the study area consisting of Jakarta, Riau, Palembang, and Jambi have shown a relatively lower CO concentration. This is the combined effect of wetter dry season and the impact of lockdown implemented by Indonesia which can be seen in Figure 5(b–e). Partial lockdown was implemented in Indonesia and was imposed as large-scale social restrictions (LSSR) as a measure of social distancing and controlling the spread of virus (Andriani, 2020). As to counter the declaration of COVID-19 as a pandemic by the WHO, the regional government initiated to limit the movement of people such as closing down schools and workplaces, shutting down public transportation, imposing a limitation on physical worship, and social-cultural activities, and implementing “stay at home” policy as reported by Anugerah et al. (2021). Furthermore on 7 January 2021, Indonesian regions introduced the Community Activities

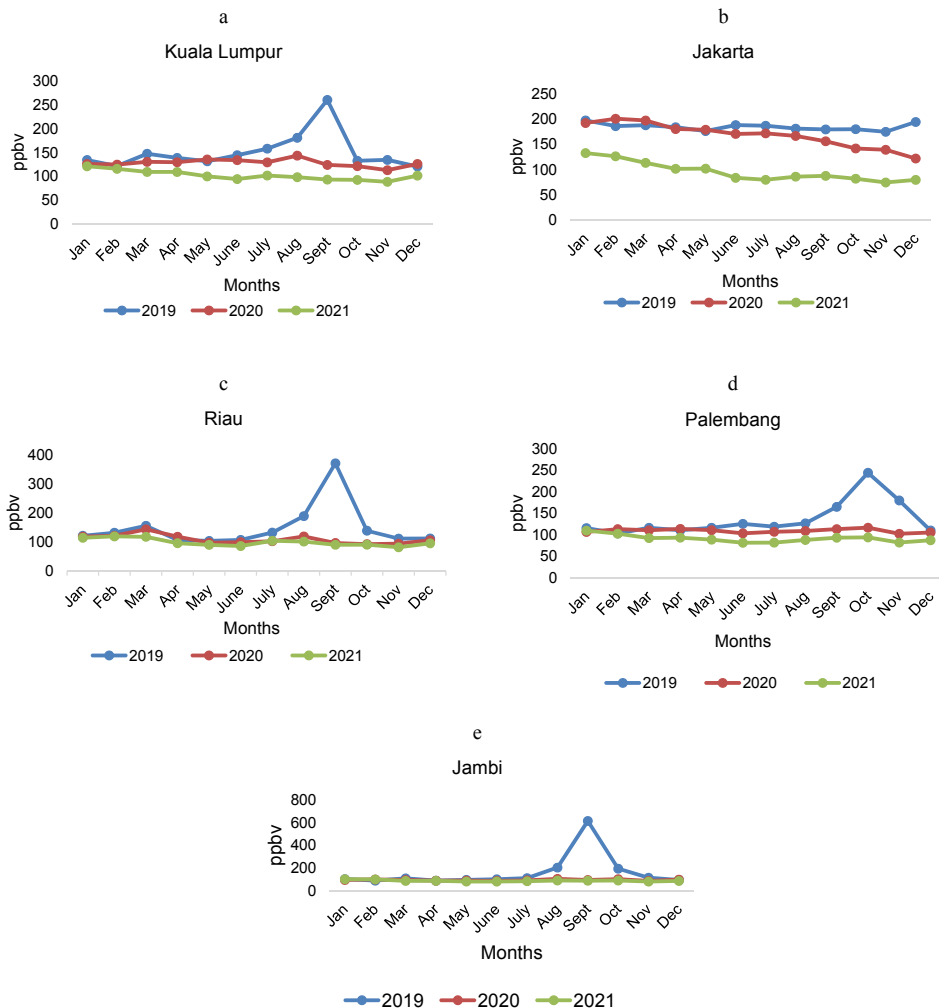


FIGURE 5. Monthly readings of CO surface concentration in ppbv (ESEMBLE) time series over (a) Kuala Lumpur, (b) Jakarta, (c) Riau, (d) Palembang, (e) Jambi before COVID-19 pandemic (2019) and during COVID-19 pandemic (2020 and 2021)

Restrictions Enforcement in some red zone areas, including the capital Jakarta and East Java province, in response to the second wave of coronavirus spread.

As both Malaysia and Indonesia are battling a second wave of coronavirus infections. Jong (2021) observed a decreasing trend for CO concentration in Indonesia

in the year 2021. The author also reported that the official data showed fire burnings of 35,271 ha of land from January to May 2021, a 9% decrease from the same period in 2020. This indicates that a reduction in CO concentration after the period of enforced lockdown is mainly due the absence of large-scale forest fires in this study regions

during COVID-19 pandemic (2020 and 2021). During the COVID-19 pandemic, the power requirements of the manufacturing sector, transportation, automobiles, industrial activities, and electricity generation also had declined, which in turn influenced the usual CO emission.

Conclusions

This paper has reviewed the effect of lockdown to CO concentration over Malaysia and Indonesia during pandemic COVID-19. MERRA-2 dataset provided by Giovanni interface was used to analyse CO surface concentration over Malaysia and Indonesia for a period of 10 years from January 2011 to December 2021. Five affected areas which are, Kuala Lumpur, Jambi, Riau, Palembang, and Jakarta were found to have higher CO value during the study period. The month of September 2019 is found to have the highest trend of CO concentration over Jambi region. The increase of CO concentrations is mostly due to the common occurrence of forest fire during the drought season which has been identified as the main source of CO emissions. As COVID-19 pandemic hit the whole world at the end of 2019, all the studied regions showed a decreasing trend after September 2019 and no high peak was observed throughout the year 2020 and 2021. This is the combined effect of wetter dry season, absence of large-scale forest fire and the impact of lockdown implemented by the both governments of Malaysia and Indonesia.

Acknowledgement

We would like to thank Universiti Teknologi MARA Cawangan Terengganu, Kampus Bukit Besi management for their

support and encouragement. We also acknowledge the MODIS mission scientists and associated NASA personnel for the production of the data used in this research effort. Analysis and visualizations used in this paper were produced with the Giovanni online data system, developed and maintained by the NASA GES DISC.

References

- Andriani, H. (2020). Effectiveness of large-scale social restrictions (PSBB) toward the new normal era during COVID-19 outbreak: a mini policy review. *Journal of Indonesian Health Policy and Administration*, 5 (2), 61–65.
- Anugerah, A. R., Muttaqin, P. S. & Purnama, D. A. (2021). Effect of large-scale social restriction (PSBB) during COVID-19 on outdoor air quality: Evidence from five cities in DKI Jakarta Province, Indonesia. *Environmental Research*, 197, 111164. <https://doi.org/10.1016/j.envres.2021.111164>
- Azhari, A., Mohamed, A. F. & Latif, M. T. (2016). Carbon emission from vehicular source in selected industrial areas in Malaysia. *International Journal of the Malay World and Civilisation*, 4 (1), 89–93.
- BBC News (2019-10-16). *Indonesia haze: Why do forests keep burning?* Retrieved from: <https://www.bbc.com/news/world-asia-34265922>
- Collivignarelli, M. C., Abbà, A., Bertanza, G., Pedrazzani, R., Ricciardi, P. & Miino, M. C. (2020). Lockdown for CoViD-2019 in Milan: What are the effects on air quality? *Science of the Total Environment*, 732, 139280. <https://doi.org/10.1016/j.scitotenv.2020.139280>
- Fisher, J. A., Iscoe, S., Fedorko, L. & Duffin, J. (2011). Rapid elimination of CO through the lungs: coming full circle 100 years on. *Experimental Physiology*, 96 (12), 1262–1269. <https://doi.org/10.1113/exp-physiol.2011.059428>
- Freedman, A. (2019-09-23). *Skies turn red across parts of Indonesia as crisis from fire-induced haze escalates*. Washington Post. Retrieved from: <https://www.wash->

- ingtonpost.com/weather/2019/09/23/skies-turn-red-across-parts-indonesia-crisis-fire-induced-haze-escalates
- Gelaro, R., McCarty, W., Suárez, M. J., Todling, R., Molod, A., Takacs, L., Randles, C. A., Darmenov, A., Bosilovich, M. G., Reichle, R. & Wargan, K. (2017). The modern-era retrospective analysis for research and applications, version 2 (MERRA-2). *Journal of Climate*, 30 (14), 5419–5454.
- Harris, S. (2020-03-22). *Around the world, daily life comes to a near-halt as more governments impose restrictions on movement*. Washington Post. Retrieved from: https://www.washingtonpost.com/national/around-the-world-daily-life-comes-to-a-near-halt-as-more-governments-impose-restrictions-on-movement/2020/03/22/39c4c12e-6b88-11ea-abef-020f086a3fab_story.html
- Jong, H. N. (202-07-21). *Indonesia eyes less severe fire season, but COVID-19 could turn it deadly*. Mongabay. Retrieved from: <https://news.mongabay.com/2021/07/indonesia-eyes-less-severe-fire-season-but-covid-19-could-turn-it-deadly>
- Kamarudin, W. F. W., Muhammad, A., Sa'ad, F. N. A. & Mustapha, R. I. P. R. (2019). Spatial and temporal CO concentration over Malaysia and Indonesia using 4 decades remote sensing dataset. *TEM Journal*, 8 (3), 836. <https://doi.org/10.18421/TEM83-20>
- Kerimray, A., Baimatova, N., Ibragimova, O. P., Bukenov, B., Kenessov, B., Plotitsyn, P. & Karaca, F. (2020). Assessing air quality changes in large cities during COVID-19 lockdowns: The impacts of traffic-free urban conditions in Almaty, Kazakhstan. *Science of the Total Environment*, 730, 139179. <https://doi.org/10.1016/j.scitotenv.2020.139179>
- Kiki, S. (2019-10-07). *Fighting haze-causing forest fires in Indonesia's Jambi province*. Channel News Asia. Retrieved from: <https://www.channelnewsasia.com/news/asia/fighting-haze-causing-forest-fires-in-indonesia-s-jambi-province-11976620>
- Lavorel, S., Flannigan, M. D., Lambin, E. F. & Scholes, M. C. (2007). Vulnerability of Land Systems to Fire: Interactions Among Humans, Climate, the Atmosphere, and Ecosystems. *Mitigation and Adaptation Strategies for Global Change*, 12 (1), 33–53.
- Mahato, S., Pal, S. & Ghosh, K. G. (2020). Effect of lockdown amid COVID-19 pandemic on air quality of the megacity Delhi, India. *Science of the Total Environment*, 730, 139086. <https://doi.org/10.1016/j.scitotenv.2020.139086>
- Manisalidis, I., Stavropoulou, E., Stavropoulos, A. & Bezirtzoglou, E. (2020). Environmental and health impacts of air pollution: a review. *Frontiers in Public Health*, 8, 1–13. <https://doi.org/10.3389/fpubh.2020.00014>
- Nadzir, M. S. M., Ooi, M. C. G., Alhasa, K. M., Bakar, M. A. A., Mohtar, A. A. A., Nor, M. F. F. M., Latif, M. T., Hamid, H. H. A., Ali, S. H. M., Ariff, N. M., Anuar, J., Ahamad, F., Azhari, A., Hanif, N. M., Subhi, M. A., Othman, M. & Nor, M. Z. M. (2020). The impact of movement control order (MCO) during pandemic COVID-19 on local air quality in an urban area of Klang valley, Malaysia. *Aerosol and Air Quality Research*, 20 (6), 1237–1248.
- Perutz, M. F. (1990). Mechanisms regulating the reactions of human hemoglobin with oxygen and carbon monoxide. *Annual Review of Physiology*, 52 (1), 1–26.
- Rajab, J. M., Tan, K. C., Lim, H. S. & Mat Jafri, M. Z. (2011). Investigation on the Carbon Monoxide Pollution over Peninsular Malaysia Caused by Indonesia Forest Fires from AIRS Daily Measurement. *Advanced Air Pollution/Book, 1*, 115–136.
- Rana, A. D., Ali, M., Mahmood, K., Tariq, S. & Qayyum, Z. (2015). Carbon monoxide (CO) emissions and its tropospheric variability over Pakistan using satellite-sensed data. *Advances in Space Research*, 56 (4), 583–595.
- Taufik, K. (2020). *Commentary: Little smoke this haze season – but fires rage on in Indonesia*. Retrieved from: Channel News Asia. <https://www.channelnewsasia.com/news/commentary/indonesia-forest-fire-peat-haze-palm-oil-jokowi-omnibus-bill-13533700>
- World Health Organization [WHO] (2021). *WHO Coronavirus (COVID-19 Dashboard)*. Retrieved from: <https://covid19.who.int>

Summary

Lockdown effect on carbon monoxide concentration over Malaysia and Indonesia. An increase in Indonesian forest fires has infuriated Malaysia and Indonesia, where residents are inhaling smoke from peat and trees burned hundreds of miles away. The global COVID-19 lockdowns caused carbon monoxide (CO) emissions decreased seen over Malaysia and Indonesia regions. The main objective of this study is to investigate the CO distribution over Malaysia and Indonesia, within the period of January 2011 to December 2021. The impact of lockdown due to COVID-19 pandemic in 2020 and 2021 to CO concentration over Malaysia and Indonesia also was reviewed. This study utilizes MERRA-2 dataset provided

by Giovanni interface. Five areas were found to be affected the most during the study period which is Kuala Lumpur, Jambi, Riau, Palembang, and Jakarta. Carbon monoxide concentration over the studied region exhibits a strong seasonality showing maximum value in dry season (July to October). September 2019 is found to have the highest trend of CO concentration affected Jambi region. As COVID-19 pandemic hit the whole world by end of year 2019, all the studied regions shown the decreasing trend after September 2019 and no high peak was observed during dry season (July to October) in 2020 and 2021. This is the combined effect of wetter dry season and an impact of lockdown implemented by government of Malaysia and Indonesia.

Hanane SLIMANI✉

Akila ABDI

Zidane BRANES

Badji Mokhtar Annaba University, Faculty of Sciences, Algeria

ISOLATION, CHARACTERIZATION AND GROWTH ASSESSMENT OF BIODEGRADING CHLORPYRIFOS-METHYL *BACILLUS* SPECIES ISOLATED FROM ALGERIAN SOIL

Key words: chlorpyrifos-methyl, Algerian agriculture lands, *Bacillus* genus, bacterial growth, bioremediation, soil pollution

Introduction

Pesticides incorporate a broad spectrum of chemicals, including insecticides, fungicides, molluscicides, rodenticides, nematocides, plant growth regulators, weedicides, etc. (Aktar, Sengupta & Chowdhury, 2009). The increasing exponential growth of the world's population is generating a huge use of pesticides in the world to fulfill the augmenting needs for food and fibers (Foong et al., 2020). Agricultural yield has been rising due to the application of pesticides, controlling pests, diseases and helping to

keep many dreaded diseases away from society (Naik & Prasad, 2006). However, the overuse of pesticides is proving to be one of the major obstacles to sustainable agricultural production (Agarwal & Pandey, 2017). At present, organophosphates (OPs) are the most widely used pesticides in agriculture due to their lower persistence in the environment and higher efficacy compared to organochlorine and carbamate pesticides (Das & Adhya, 2015; Foong et al., 2020).

Organophosphates are mainly esters, thiols, or amide derivatives of phosphoric or phosphoramidic acids with two organic groups and an additional side chain (Kumar, Kaushik & Villarreal-Chiu, 2016). On the whole, OPs account for more than 36% of the total worldwide sales market (Briceño et al., 2012).

Chlorpyrifos-methyl (o,o-dimethyl-o-(3,5,6-trichloro-2-pyridyl) phosphorothioate, is a broad-spectrum organophosphate insecticide that is widely used in pest control (Choi & Lee, 2016; Szpyrka, Matyaszek & Słowik-Borowiec, 2017). Although chlorpyrifos-methyl insecticides as well as other OPs are relatively less persistent in the environment and less toxic to non-target animals, their over application and high use frequency can lead to high levels of OP and chlorpyrifos-methyl residues on agricultural products including agricultural crops/fruits, pond/canal water/wells, and many others, which could have negative environmental and public health effects (Matthews, 1990; Abbassy, Salim, Shawir & Nassar, 2017; Bose, Kumar & Vo, 2021). These issues emphasize the necessity of removing chlorpyrifos-methyl residues from contaminated soils, water systems, and crops. Microbial degradation has been found to be the most prominent bioremediation method, as it is the major factor impacting chlorpyrifos-methyl degradation (Kim & Ahn, 2009).

Algeria is currently classified among the countries that use huge quantities of pesticides. There are about 400 registered phytosanitary products in Algeria, of which about 40 varieties are widely used by farmers (Bouziani, 2007). Unfortunately, the determination of the level of contamination of natural compartments is not done systematically. Analyses carried out on water samples taken in the region of Staouli (Algiers Province) and Annaba have shown that in more than 30% of the samples, the concentration of certain organochlorine and organophosphorus molecules exceeds the values recommended by the World Health Organization (WHO). The national use of phytosanitary products in agronomy makes fear a massive pollution of soils,

surface waters, water tables and all physical environments in all regions of the country, leading to serious health problems.

Among the remediation technologies proposed for contaminated ecosystems, bioremediation is recognized as one of the most prospective approaches. It is a comparatively inexpensive, simple to use, and environmentally friendly technique (Rayu, Karpousas & Singh, 2012; Huang et al., 2021). The use of microorganisms with the right metabolic pathways is one of the most sustainable alternatives for chlorpyrifos-methyl remediation. To date, a few chlorpyrifos-methyl-degrading bacteria have been isolated from the environment, but studies of these bacteria generally focus only on the concentration of chlorpyrifos-methyl in the biodegradation process, and there is minimal understanding of degradation intermediates and degradation mechanisms (Rayu, Nielsen, Nazaries & Singh, 2017). Excessive use of the pesticide and its accumulation in the soil can change the physicochemical properties of soil.

The aim of this study is to isolate indigenous bacterial strains from agricultural soils located in northeastern Algeria, and to assess their ability to grow in the presence of chlorpyrifos-methyl as the sole source of energy and carbon. Thus, their growth would make it possible to consider the use of high-performance strains as a means of bioremediation and biodegradation.

Material and methods

Soil sampling

For this work, three experimental agricultural stations, where they were exposed to the application of CM for long

time periods, were selected to isolate CM degrading strains. Samples were collected in the top layer of 0–25 cm from each station. These sites were located at the Technical Institute of Vegetable and Industrial Crops (TIVIC), El Tarf Province located in the far North-East of Algeria. Samples that served for microbiological analysis were collected in sterilized Erlenmeyer of 500 ml capacity, and then conserved at 4°C till use.

Isolation and, identification of soil indigenous bacterial strains

The technique for isolating soil autochthonous bacteria was performed as described by (Aswathi, Pandey & Sukumaran, 2019). Ten grams of each soil sample was added to 90 ml of sterile physiological water and the suspension was gently agitated (150 rpm) at room temperature for approximately 30 min. Decimal dilutions of 10^{-1} – 10^{-6} were prepared using sterile physiological water. One-milliliter aliquots were transferred to sterile Petri dishes and held for 10 min before adding Luria–Bertani (LB) agar medium. Plates were incubated at 30°C for 18–24 h, and colonies were purified on LB agar.

Bacterial isolates were identified by using standard methods: morphological identification, Gram staining, oxidase, catalase as well as biochemical tests by using API 20E, API 20NE, API Staph galleries (bioMérieux Inc., France), as well as a molecular method. The PCR amplification and sequencing of genomic DNA for 16s rRNA using universal primers 27f (5'-AGAGTTTGATCMTGGCT-CAG-3') and 1492r (5'-TACGGYTACCTT-GTTACGACTT-3') was performed in a PCR thermocycler instrument with the following cyclic profile: initial denaturation at 95°C for 5 min, 35 cycles of denaturation at 95°C for

30 s, annealing at 52°C for 30 s, extension at 72°C for 1 min 30 s and final extension at 72°C for 5 min (Batisson et al., 2009). The determined 16S rRNA gene (partial sequence) was aligned with those available in the GenBank database.

Following multiple alignments of the sequence data using ClustalX, phylogenetic analysis was performed using the MEGA 5.0 software packages (Thompson, Gibson, Plewniak, Jeanmougin & Higgins, 1997). Phylogenetic trees were generated using the neighbor-joining method according to the maximum composite likelihood parameter model and evaluated by bootstrap analyses based on 1,000 resembling (Tamura et al., 2011).

A mineral salt medium (MSM) was employed for both strain selection and biodegradation trials of CM-degrading strains. This medium contained per liter of distilled water: 1.6 g K_2HPO_4 , 1.6 g KH_2PO_4 , 0.2 g $MgSO_4 \cdot 7H_2O$, 1 g NaCl, 0.02 g $CaCl_2$, 3.5 g $(NH_4)_2SO_4$, 1 ml of $FeSO_4 \cdot 6H_2O$ -EDTA. The pH was adjusted at 7.5. A solid MSM obtained by adding 15 g $\cdot l^{-1}$ agar was used to test the capacity of the strains to grow on a solid medium (Rousseaux, Hartmann & Soulas, 2001).

Screening for CM degrading-bacterium

The selection test was based on evaluating bacterial growth on MSM agar plates supplemented with a concentration of CM as the only carbon and energy source. Chlorpyrifos-methyl was sterilized by 0.45 μm membrane filtration and added to the medium to obtain the required concentrations of 25, 50, 100 and 200 $mg \cdot l^{-1}$. Plates were incubated in the dark at 30°C for 24 h to 15 days. Strains were then rated as negative and positive growth. Bacterial strains that

had shown higher growth on MSM agar were then tested for CM biodegradation in MSM liquid media (Pankaj et al., 2016).

Bacterial growth in MSM liquid media

A suspension of the isolates of interest was made by transferring a few pure bacterial colonies into sterile physiological water. Growth assays with CM as the only carbon and energy source were performed in sterile 500 ml Erlenmeyer flasks containing 100 ml of sterile MSM broth. The CM was introduced as a stock solution to have a dose of $50 \text{ mg} \cdot \text{l}^{-1}$. The Erlenmeyer flasks were incubated at $30^\circ\text{C} \pm 2^\circ\text{C}$ in an incubator with shaking at 150 rpm under aerobic conditions and protected from light. Samples of the liquid medium were taken in a sterile manner at different time intervals to measure the bacterial concentration which was determined by monitoring the optical density (OD) at 600 nm using a UV spectrophotometer (Secomam Uviline, 9000). Samples without pesticides were used as abiotic controls. All measurements were performed in triplicate (Uniyal, Sharma & Kondakal, 2021).

Results and discussion

Screening and characterization of CM-degrading bacteria

Pesticides are degraded by microorganisms that utilize them as carbon sources and electron donors. However, their degradation depends on various environmental factors and on physiological, ecological, biochemical and molecular aspects. Microorganisms with the potential to degrade pesticides have been isolated and characterized in different laboratories around the world. However,

the molecular technology of DNA sequencing has expanded our understanding of the mechanisms, occurrence and identification of effective microorganisms for bioremediation of polluted ecosystems (Ortiz-Hernández, Sánchez-Salinas, Dantán-González & Castrejón-Godínez, 2013).

In our research, several strains between Gram-positive and Gram-negative were isolated from the three agricultural stations. Among them, several strains had the ability to grow on MSM agar supplemented with increasing doses of CM that has been used as the sole source of carbon and energy. As a result, four bacterial strains showed the best growth capacity at $50 \text{ mg} \cdot \text{l}^{-1}$ of CM, in which the strains has been coded as and MC09 (Tables 1 and 2). Such strains were therefore selected for the growth test on liquid MSM.

TABLE 1. Results of the growth test of strains according to their development capacity on MSM agar in the presence of different doses (25, 50, 100, and $200 \text{ mg} \cdot \text{l}^{-1}$) of chlorpyrifos-methyl as a sole carbon and energy source

Tested isolate	$25 \text{ mg} \cdot \text{l}^{-1}$	$50 \text{ mg} \cdot \text{l}^{-1}$	$100 \text{ mg} \cdot \text{l}^{-1}$	$200 \text{ mg} \cdot \text{l}^{-1}$
JC415	++	+	+	-
SDP1	+++	++	+	+
SDP7	++	+	-	-
S17	+++	+++	++	+
JM56	+	-	-	-
ANT02	+	+	-	-
ANT14	+++	++	+	+
MA26	+	-	-	-
MC09	+++	++	-	-
JC41	++	+/-	-	-

Microscopic, biochemical characterizations, as well as the 16S rDNA sequencing results of the isolated strains are grouped together in Table 2, which shows the biochemical characteristics of the strains tested. Thus, with the exception of the ANT14 isolate, which is catalase negative, the other strains have the same Gram-positive, catalase-positive, oxidase-positive and positive motility characteristics. Consequently, the identification of 16S rDNA revealed various species as mentioned in Table 2.

The obtained tree was drawn with the length of the branches in the same units as those of the evolutionary distances used to deduce a phylogenetic tree. The evolutionary distances were calculated using the composite maximum likelihood method and are expressed in units of the number of base substitutions per site. All positions containing gaps and missing data were removed from the dataset. Phylogenetic analyzes were carried out with MEGA 5.0 software (Tamura et al., 2011). The identified species belong to two very close clusters (Fig. 1).

TABLE 2. Microscopic characteristics, biochemical and 16S rDNA identification of the interesting strains

Isolate	Gram	Oxydase	Catalase	Mobility	Biochemical identification	Identification 16S rDNA
SDP1	+	+	+	+	<i>Bacillus</i> sp.	<i>Bacillus</i> sp. H1-80
MC09	+	+	+	+	<i>B. brevis</i>	<i>Brevibacterium frigoritolerans</i> strain WJB99
ANT14	+	+	-	+	<i>B. thuringiensis</i>	<i>Bacillus</i> sp. strain GL5 (1 st strain)
S17	+	+	+	+	<i>B. lentus</i>	<i>Bacillus</i> sp. strain GL5 (2 nd strain)

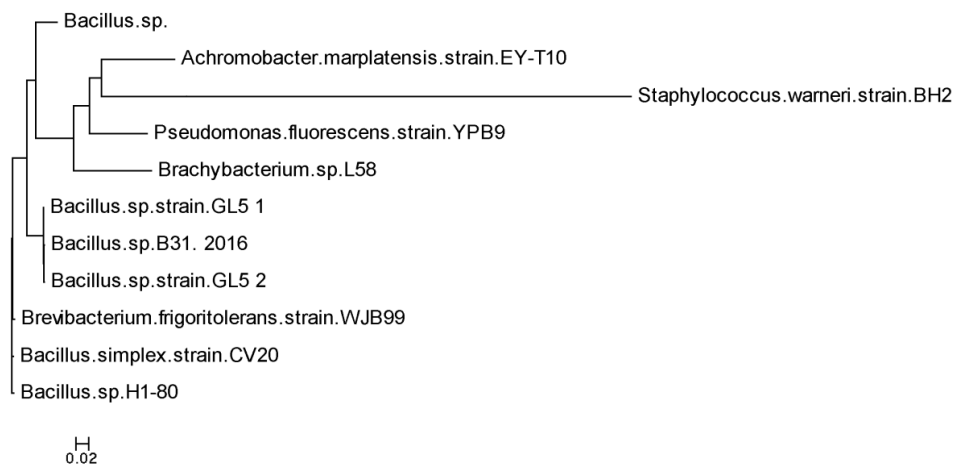


FIGURE 1. Phylogenetic tree and evolutionary relationships between the selected species

Bacterial growth in MSM liquid media supplemented with CM

Previous studies have shown the ability of microorganisms to degrade various agrochemicals while using them as a source of carbon and nitrogen (Cycoń, Żmijowska, Wójcik & Piotrowska-Seget, 2013). Thus, the demand for eco-friendly solutions and the use of indigenous species to restore pesticide-contaminated soils is growing globally. Biodegradation is considered the best option for *in-situ* restoration operations (Abigail, Samuel & Ramalingam, 2015).

The strains of interest were identified then tested in the presence of increasing concentrations of our insecticide. In the absence of alternative carbon and energy sources, the pesticide added to the solid and then liquid MSM appeared to be degraded and assimilated by our isolates during their development.

The evolution of the strains' growth was monitored by measuring absorbance

at 600 nm by spectrophotometer, over relatively long periods. Sterile samples were taken regularly in different time intervals to determine whether there is an increase or decrease in cell biomass under the experimental conditions tested. Using CM as the unique source of energy and carbon, the growth curves obtained with the *Bacillus* strains are shown on Figure 2.

Both strains of *Bacillus* sp. strain GL5 (1st and 2nd strain) reached a maximum OD after 360 and 336 h, respectively (Figs 2 and 3). This phase means high-speed acclimatization of the bacteria with their new conditions of development in the laboratory, that is, there was a real consumption of the active substance available in the medium by our microorganisms.

As we noticed, the obtained curves have a special aspect (absence of stationary phase leading to a bell shape). These isolates show a very particular and characteristic growth. Also, it was demonstrated that the maximum growth of the bacterial cells differs from one

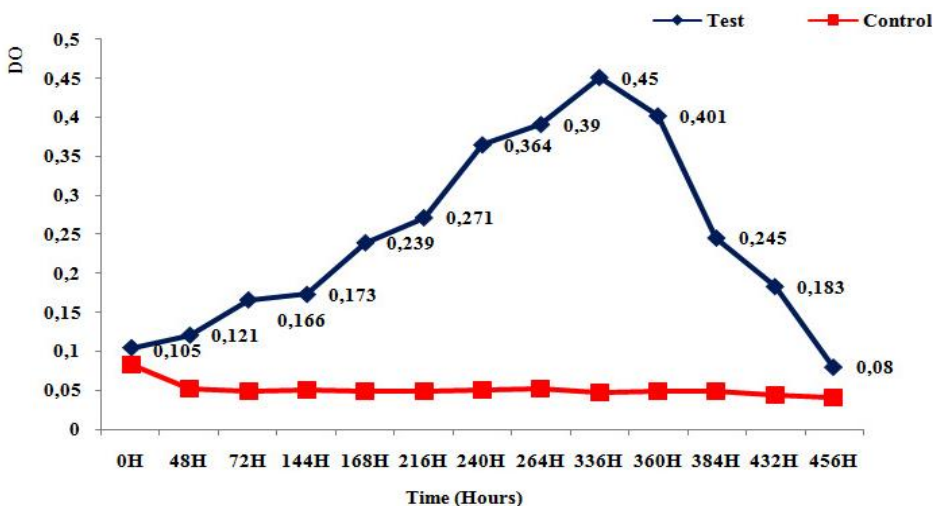


FIGURE 2. Growth of *Bacillus* sp. strain GL5 (1st strain) in the presence of 50 mg·l⁻¹ of CM as the unique source of carbon and energy

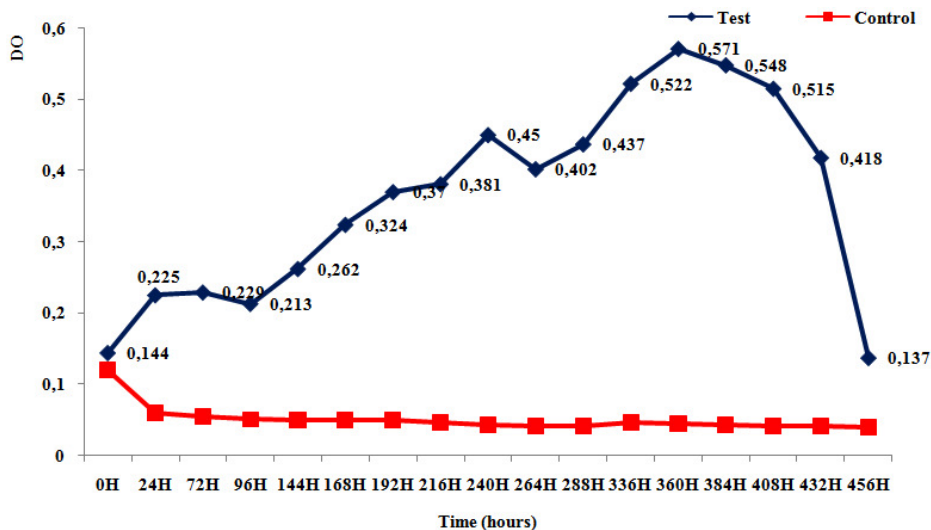


FIGURE 3. Growth of *Bacillus* sp. strain GL5 (2nd strain) in the presence of 50 mg·l⁻¹ of CM as the unique source of carbon and energy

strain to another. The absence of a latent phase in the growth curves seems to justify the interesting behavior of *Bacillus* strains with CM.

The appearance of the curves revealed a clear acceleration and duplication of the cell quantities until reaching a maximum absorbance after 48 h of incubation only

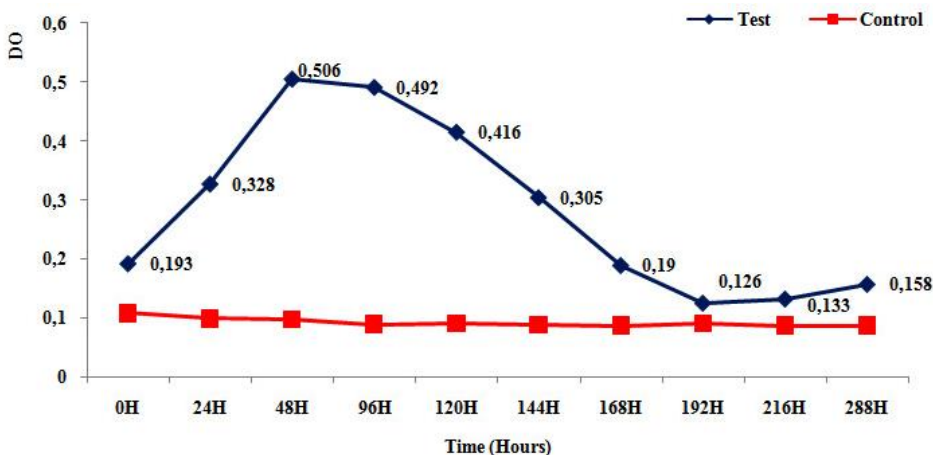


FIGURE 4. Growth of *Bacillus* sp. H1-80 in the presence of 50 mg·l⁻¹ of CM as the unique source of carbon and energy

for *Bacillus* sp. H1-80 (Fig. 4), and 72 h for *Brevibacterium frigoritolerans* strain WJB99 (Fig. 5).

Finally, a common decrease of the optical density in all the species was noted. This stage of growth corresponds to the phase of cellular decline, which is likely linked to possible cell lysis and a lack of substrate in the culture medium.

The slight decline of OD observed with *Brevibacterium frigoritolerans* strain WJB99 (Fig. 5) and *Bacillus* sp. strain GL5 (2nd strain) (Fig. 3) at the end of the 288th and 264th hour of incubation, respectively, could be explained by the production of secondary metabolites more toxic than the starting molecule, thus affecting bacterial growth. Interestingly, these curves showed that no toxic effect on the growth of bacterial cells was observed, and CM has been easily used as an energy source. It should be noted that no previous studies have been

conducted on the biodegradation of CM by the bacterium *Brevibacterium frigoritolerans* strain WJB99.

Previous works have already described the resistance of chlorpyrifos to degradation (Mallick, Bharati, Banerji, Shakil & Sethunathan, 1999). Subsequently, studies identified bacteria belonging to the genera *Enterobacter* (Singh, Walker, Morgan & Wright, 2004), *Pseudomonas* (Farhan, Khan, Wahid, Ahmad & Ahmad, 2012), *Bacillus* (Liu, Chen, Shi & Su, 2012; El-Helow, Badawy, Mabrouk, Mohamed & El-Beshlawy, 2013), *Klebsiella* (Ghanem, Orfi & Shamma, 2007) were effectively exhibiting the ability to degrade chlorpyrifos. Other recent investigations state the diversity of chlorpyrifos-degrading bacteria including *Bacillus* (Anwar, Liaquat, Khan, Khalid & Iqbal, 2009). The latter could use as a source of carbon and energy and degrade 3,5,6-trichloropyridinol (TCP),



FIGURE 5. Growth of *Brevibacterium frigoritolerans* strain WJB99 in the presence of 50 mg l⁻¹ of CM as the unique source of carbon and energy

a metabolite that is more toxic than CM itself and moderately mobile in the soil.

Many reviews and works have highlighted the importance of *Bacillus* species in the biodegradation and bioremediation of pesticides, especially chlorpyrifos. Maya, Singh, Upadhyay and Dubey (2011) studied the rate of chlorpyrifos biodegradation by three microorganisms of which *Bacillus* sp. were able to remove 52% of the tested doses during ten days. Another study revealed the capability of *Bacillus cereus* to degrade up to 74% of chlorpyrifos with an initial concentration of $100 \text{ mg}\cdot\text{l}^{-1}$ (Liu et al., 2012). Furthermore, *Bacillus pumilis* C2A1 strain isolated by Anwar et al. (2009) from a cotton crop in Pakistan showed its significant ability to metabolize high doses of CM under different conditions, in addition to TCP at 100, 200, and $300 \text{ mg}\cdot\text{l}^{-1}$ corresponding respectively to 73, 83 and 87% in liquid medium for ten days.

The diversity of our data observed with the isolated microorganisms is directly linked with the capacity of the soil microflora to adapt to a given pesticide. Generally, the phenomenon of acclimatization and biodegradation occurs when a phytosanitary product is placed in contact with an agricultural plot. This is expressed by a decomposition of the active substance after a very variable duration according to the nature of the product, called the latent period. This first step represents the enzymatic induction that can be described by a physiological and/or genetic adaptation of the microbial populations in question. During a second phase, the degradation of the active substance often results in an exponential decrease of the residual concentration. In case of frequent and successive application of the same product, plus the presence of a very high density of adapted microbial strains, the duration of

the latency phase will decrease or even be eliminated. In this case, in adapted soils, 80% of the applied phytosanitary product can be rapidly biodegraded in less than 15 days (Devers-Lamrani, 2008).

Conclusion

In our research, four strains of *Bacillus* degrading chlorpyrifos-methyl were isolated and identified from Algerian agricultural soils exposed to different treatments by different families of phytosanitary products. These are the strains, *Bacillus* sp. strain GL5 (1), *Bacillus* sp. strain GL5 (2), *Bacillus* sp. H1-80 and *Brevibacterium frigoritolerans* strain WJB99 which showed good growth on liquid medium containing $50 \text{ mg}\cdot\text{l}^{-1}$ of MC as sole carbon source. Depending on the duration of growth, *Bacillus* sp. H1-80 and *Brevibacterium frigoritolerans* strain WJB99 are the most efficient with respectively a maximum of OD after 48 and 72 h of growth. In perspective, optimization studies would be interesting to carry out as well as the sequencing of CM degradation genes, since our strains have not been cited in previous work. Given the high growth capacity of the strains in the presence of CM, they could be very useful for the bioremediation of soils contaminated by this insecticide.

References

- Abbassy, M. A., Salim, Y. M. M., Shawir, M. S. & Nassar, A. M. K. (2017). Disappearance and hazard quotient of chlorpyrifos-methyl, fipronil, and imidacloprid insecticides from dates. *Journal of Consumer Protection and Food Safety*, 12 (3), 223–230.
- Abigail, M. E. A., Samuel, S. M. & Ramalingam, C. (2015). Addressing the environmental impacts

- of butachlor and the available remediation strategies: a systematic review. *International Journal of Environmental Science and Technology*, 12 (12), 4025–4036.
- Agarwal, P. K. & Pandey, D. I. V. Y. A. (2017). Impact of pesticide: an overview. *Trends in Bioscience*, 10 (6), 1341–1344.
- Aktar, M. W., Sengupta, D. & Chowdhury, A. (2009). Impact of pesticides use in agriculture: their benefits and hazards. *Interdisciplinary Toxicology*, 2 (1), 1–2.
- Anwar, S., Liaquat, F., Khan, Q. M., Khalid, Z. M. & Iqbal, S. (2009). Biodegradation of chlorpyrifos and its hydrolysis product 3,5,6-trichloro-2-pyridinol by *Bacillus pumilus* strain C2A1. *Journal of Hazardous Materials*, 168 (1), 400–405.
- Aswathi, A., Pandey, A. & Sukumaran, R. K. (2019). Rapid degradation of the organophosphate pesticide – Chlorpyrifos by a novel strain of *Pseudomonas nitroreducens* AR-3. *Bioresource Technology*, 292, 122025. <https://doi.org/10.1016/j.biortech.2019.122025>
- Batissou, I., Crouzet, O., Besse-Hoggan, P., Sancelme, M., Mangot, J. F., Mallet, C. & Bohatier, J. (2009). Isolation and characterization of mesotrione-degrading *Bacillus* sp. from soil. *Environmental Pollution*, 157 (4), 1195–1201.
- Bose, S., Kumar, P. S. & Vo, D. V. N. (2021). A review on the microbial degradation of chlorpyrifos and its metabolite TCP. *Chemosphere*, 283, 131447. <https://doi.org/10.1016/j.chemosphere.2021.131447>
- Bouziani, M. (2007). *The immoderate use of pesticide. Serious health consequences. The guide of medicine and health. Maghreb Health*. Retrieved from: <https://santetropicale.com/santemag/algerie/poivue51.htm>
- Briceño, G., Fuentes, M. S., Palma, G., Jorquera, M. A., Amoroso, M. J. & Diez, M. C. (2012). Chlorpyrifos biodegradation and 3,5,6-trichloro-2-pyridinol production by actinobacteria isolated from soil. *International Biodeterioration & Biodegradation*, 73, 1–7.
- Choi, W. S. & Lee, S. E. (2016). Toxicity of chlorpyrifos-methyl to *Sitophilus zeamais* collected in Korea and biochemical differences. *Entomological Research*, 46 (1), 15–22.
- Cycoń, M., Żmijowska, A., Wójcik, M. & Piotrowska-Seget, Z. (2013). Biodegradation and bioremediation potential of diazinon-degrading *Serratia marcescens* to remove other organophosphorus pesticides from soils. *Journal of Environmental Management*, 117, 7–16.
- Das, S. & Adhya, T. K. (2015). Degradation of chlorpyrifos in tropical rice soils. *Journal of Environmental Management*, 152, 36–42.
- Devers-Lamrani, M. (2008). *Study of the mechanisms at the origin of the dispersion of the genes encoding the enzymes responsible for the mineralization of atrazine within the soil microflora* (PhD thesis). French National Institute for Agricultural Research, Dijon.
- El-Helow, E. R., Badawy, M. E., Mabrouk, M. E., Mohamed, E. A. & El-Beshlawy, Y. M. (2013). Biodegradation of chlorpyrifos by a newly isolated *Bacillus subtilis* strain, Y242. *Bioremediation Journal*, 17 (2), 113–123.
- Farhan, M., Khan, A. U., Wahid, A., Ahmad, M. & Ahmad, F. (2012). Biodegradation of chlorpyrifos using indigenous *Pseudomonas* sp. isolated from industrial drain. *Pakistan Journal of Nutrition*, 11 (12), 1183. <https://doi.org/10.3923/pjn.2012.1183.1189>
- Foong, S. Y., Ma, N. L., Lam, S. S., Peng, W., Low, F., Lee, B. H., Alstrup, A. K. O. & Sonne, C. (2020). A recent global review of hazardous chlorpyrifos pesticide in fruit and vegetables: prevalence, remediation and actions needed. *Journal of Hazardous Materials*, 400, 123006. <https://doi.org/10.1016/j.jhazmat.2020.123006>
- Ghanem, I., Orfi, M. & Shamma, M. (2007). Biodegradation of chlorpyrifos by *Klebsiella* sp. isolated from an activated sludge sample of waste water treatment plant in damascus. *Folia Microbiologica*, 52 (4), 423–427.
- Huang, Y., Zhang, W., Pang, S., Chen, J., Bhatt, P., Mishra, S. & Chen, S. (2021). Insights into the microbial degradation and catalytic mechanisms of chlorpyrifos. *Environmental Research*, 194, 110660. <https://doi.org/10.1016/j.envres.2020.110660>
- Kim, J. R. & Ahn, Y. J. (2009). Identification and characterization of chlorpyrifos-methyl and 3,5,6-trichloro-2-pyridinol degrading *Burkholderia* sp. strain KR100. *Biodegradation*, 20 (4), 487–497.
- Kumar, S., Kaushik, G. & Villarreal-Chiu, J. F. (2016). Scenario of organophosphate pol-

- lution and toxicity in India: a review. *Environmental Science and Pollution Research*, 23 (10), 9480–9491.
- Liu, Z. Y., Chen, X., Shi, Y. & Su, Z. C. (2012). Bacterial degradation of chlorpyrifos by *Bacillus cereus*. *Advanced Materials Research*, 356, 676–680.
- Mallick, K., Bharati, K., Banerji, A., Shakil, N. A. & Sethunathan, N. (1999). Bacterial degradation of chlorpyrifos in pure cultures and in soil. *Bulletin of Environmental Contamination and Toxicology*, 62 (1), 48–54.
- Matthews, W. A. (1990). The fate of chlorpyrifos-methyl in stored wheat: A comparison of a laboratory-scale experiment with a pilot-scale treatment. *Pesticide Science*, 30 (1), 21–29.
- Maya, K., Singh, R. S., Upadhyay, S. N. & Dubey, S. K. (2011). Kinetic analysis reveals bacterial efficacy for biodegradation of chlorpyrifos and its hydrolyzing metabolite TCP. *Process Biochemistry*, 46 (11), 2130–2136.
- Naik, S. N. & Prasad, R. (2006). Pesticide residue in organic and conventional food-risk analysis. *Journal of Chemical Health & Safety*, 13 (6), 12–19.
- Ortiz-Hernández, M. L., Sánchez-Salinas, E., Dantán-González, E. & Castrejón-Godínez, M. L. (2013). *Pesticide biodegradation: mechanisms, genetics and strategies to enhance the process. Biodegradation – Life of Science*. <https://doi.org/10.5772/56098>
- Pankaj, Sharma, A., Gangola, S., Khati, P., Kumar, G. & Srivastava, A. (2016). Novel pathway of cypermethrin biodegradation in a *Bacillus* sp. strain SG2 isolated from cypermethrin-contaminated agriculture field. *3 Biotech*, 6 (1), 1–11.
- Rayu, S., Karpouzas, D. G. & Singh, B. K. (2012). Emerging technologies in bioremediation: constraints and opportunities. *Biodegradation*, 23 (6), 917–926.
- Rayu, S., Nielsen, U. N., Nazaries, L. & Singh, B. K. (2017). Isolation and molecular characterization of novel chlorpyrifos and 3,5,6-trichloro-2-pyridinol-degrading bacteria from sugarcane farm soils. *Frontiers in Microbiology*, 8, 518. <https://doi.org/10.3389/fmicb.2017.00518>
- Rousseaux, S., Hartmann, A. & Soulas, G. (2001). Isolation and characterisation of new Gram-negative and Gram-positive atrazine degrading bacteria from different French soils. *FEMS Microbiology Ecology*, 36 (2–3), 211–222.
- Uniyal, S., Sharma, R. K. & Kondakal, V. (2021). New insights into the biodegradation of chlorpyrifos by a novel bacterial consortium: process optimization using general factorial experimental design. *Ecotoxicology and Environmental Safety*, 209, 111799. <https://doi.org/10.1016/j.ecoenv.2020.111799>
- Singh, B. K., Walker, A., Morgan, J. A. W. & Wright, D. J. (2004). Biodegradation of chlorpyrifos by *Enterobacter* strain B-14 and its use in bioremediation of contaminated soils. *Applied and Environmental Microbiology*, 70 (8), 4855–4863.
- Szpyrka, E., Matyaszek, A. & Słowik-Borowiec, M. (2017). Dissipation of chlorantraniliprole, chlorpyrifos-methyl and indoxacarb–insecticides used to control codling moth (*Cydia pomonella* L.) and leafrollers (*Tortricidae*) in apples for production of baby food. *Environmental Science and Pollution Research*, 24 (13), 12128–12135.
- Tamura, K., Peterson, D., Peterson, N., Stecher, G., Nei, M. & Kumar, S. (2011). MEGA5: molecular evolutionary genetics analysis using maximum likelihood, evolutionary distance, and maximum parsimony methods. *Molecular Biology and Evolution*, 28 (10), 2731–2739.
- Thompson, J. D., Gibson, T. J., Plewniak, F., Jeanmougin, F. & Higgins, D. G. (1997). The CLUSTAL_X windows interface: flexible strategies for multiple sequence alignment aided by quality analysis tools. *Nucleic Acids Research*, 25 (24), 4876–4882.

Summary

Isolation, characterization and growth assessment of biodegrading chlorpyrifos-methyl *Bacillus* species isolated from Algerian soil. Chlorpyrifos-methyl (CM) is a broad-spectrum organophosphate insecti-

cide, which is widely used in pest control. In this research, the isolation, and biochemical and molecular identification of bacterial strains obtained from three soils located in northeastern Algeria were carried out, as well as the evaluation of their ability to grow in the presence of CM. Out of 48 bacterial isolates between Gram-negative and Gram-positive identified, several were able to grow on mineral agar with at least $25 \text{ mg} \cdot \text{l}^{-1}$ of CM. Four bacteria showed the best growth

capacity, were identified as *Bacillus* sp. H1-80, *Brevibacterium frigiditolerans* strain WJB99 and two *Bacillus* sp. strains GL5. The strains were tested for their ability to grow on liquid media with CM as the sole energy and carbon source. In general, these strains showed slow but significant growth visualized by the 600 nm turbidity control, suggesting that they could be used for bioremediation applications of CM polluted soils.

Instruction for Authors

The journal publishes in English languages, peer-reviewed original research, critical reviews and short communications, which have not been and will not be published elsewhere in substantially the same form. Author of an article is required to transfer the copyright to the journal publisher, however authors retain significant rights to use and share their own published papers. The published papers are available under the terms of the principles of Open Access Creative Commons CC BY-NC license. The submitting author must agree to pay the publication charge (see Charges).

The author of submitted materials (e.g. text, figures, tables etc.) is obligated to restricts the publishing rights. All contributors who do not meet the criteria for authorship should be listed in an Acknowledgements section of the manuscript. Authors should, therefore, add a statement on the type of assistance, if any, received from the sponsor or the sponsor's representative and include the names of any person who provided technical help, writing assistance, editorial support or any type of participation in writing the manuscript.

Uniform requirements for manuscripts

The manuscript should be submitted by the Open Journal System (OJS) at <https://srees.sggw.edu.pl/about/submissions>. All figures and tables should be placed near their reference in the main text and additionally sent in a form of data files (e.g. Excel, Visio, Adobe Illustrator, Adobe Photoshop, CorelDRAW). Figures are printed in black and white on paper version of the journal (color printing is combined with an additional fee calculated on a case-by-case basis), while on the website are published in color.

The size of the manuscript should be limited up to 10 pages including overview, summary, references and figures (the manuscript more than 13 pages is unacceptable); Please set the text format in single column with paragraphs (A4 paper format), all margins to 25 mm, use the font Times New Roman, typeface 12 points and line spacing one and half.

The submitted manuscript should include the following parts:

- name and SURNAME of the author(s) – up to 5 authors
- affiliation of the author(s), ORCID Id (optional)
- title of the work
- key words
- abstract (about 500 characters)
- text of the paper divided into: Introduction, Material and Methods, Results and Discussion, Conclusions, References and Summary
- references in APA style are listed fully in alphabetical order according to the last name of the first author and not numbered; please find the details below
- post and mailing address of the corresponding author:

Author's address:

Name, SURNAME

Affiliation

Street, number, postal code, City

Country

e-mail: address@domain

- Plagiarism statement (<https://srees.sggw.edu.pl/copyright>)

Reference formatting

In the Scientific Review Engineering and Environmental Sciences the APA 6th edition style is used.

Detailed information

More information can be found: <https://srees.sggw.edu.pl>

